Functionalization of Polytetrafluoroethylene Surface using Atmospheric Pressure Plasma and Development of Photoemission-induced Atmospheric Pressure Gas Discharge

by

Sukma Wahyu Fitriani

Student ID Number: 1238002

A dissertation submitted to the
Engineering Course, Department of Engineering,
Graduate School of Engineering,
Kochi University of Technology,
Kochi, Japan

in partial fulfillment of the requirements for the degree of
Doctor of Engineering

Assessment Committee:
      Supervisor: Akimitsu Hatta
      Co-Supervisor: Hiroshi Furuta
      Co-Supervisor: Hisao Makino
      Chaoyang Li
      Mamoru Furuta

September 2022

Abstract

Functionalization of Polytetrafluoroethylene Surface using Atmospheric Pressure Plasma and Development of Photoemission-induced Atmospheric Pressure Gas Discharge

An application of dielectric barrier discharge plasma for polytetrafluoroethylene (PTFE) surface modification and a generation of novel atmospheric pressure gas discharge induced by photoemission are presented in this study. The aims are to enhance the wettability of PTFE using atmospheric pressure plasma of gaseous with water-ethanol vapor and to ignite stable atmospheric pressure gas discharge induced by photoemission using argon and air for medical and agriculture applications.

In the first part of this work, an atmospheric pressure plasma was generated by the dielectric barrier discharge of Ar or N_2 gas bubbled into a water-ethanol solution. The quadrupole mass analysis revealed that atmospheric pressure plasma promoted the decomposition of ethanol and produced H_2, CH_4, CO, and CO_2. In the case of Ar with water-ethanol plasma treatment, it was found that small ethanol concentrations in the range of 3%-9% were optimum to improve the wettability of PTFE. By using this optimum condition, water contact angle (WCA) decreased with increasing treatment time and then leveled off after 10 s of treatment from 115° (as-received PTFE) to around 20°. On the other hand, for N_2 with water-ethanol, the ethanol concentration of 5%, 9%, 50%, and 100% resulted in a similar hydrophilic surface finish, suggesting that ethanol concentration did not significantly influence the wettability of PTFE. Initially, the water contact angle decreased with increasing treatment time to around 12° after 15 s treatment, then it recovered up to around 80° when treatment time was further increased to 20 s.

The surface analysis of PTFE was performed by using an atomic force microscope for morphological examination and using an X-ray photoelectron spectroscopy (XPS) for chemical

composition measurement. However, by comparing before and after plasma treatment, the surface morphology showed less significant changes. In contrast, the XPS spectrum revealed that oxygen-containing functional groups and nitrogen-containing functional groups, namely hydroxyl, carbonyl, and carboxyl, amine, and amide groups, formed on the plasma-treated PTFE surface, reflecting the hydrophilization of PTFE. In the case of Ar with water-ethanol, at the beginning of the plasma treatment, the water vapor induced the breaking of the CF_2 chain, and the additional ethanol vapor generated oxygen-containing polar groups on the PTFE surface. In addition to the modification of the PTFE surface itself, a low-molecular-weight oxidized material (LMOWM) layer was deposited over the surface, which prevented further surface modification, and the deposited layer exhibited excellent wettability. The deposited LMWOM layer was easily removed by immersion in deionized water, and the exposed modified PTFE surface exhibited stable wettability with a WCA of $52.7 \pm 3.5°$. For N_2 with water-ethanol, the deposition of thin layer rich in polar groups was a dominant process that resulted in significant improvement of wettability. Nevertheless, severe degradation of water contact angle occurred leaving stable modification of PTFE surface around 80° of WCA.

In the second part of this study, photoemission-induced atmospheric-pressure gas discharge was successfully generated in Ar and air. A discharge cell consists of a 9 nm gold thin film deposited on quartz glass as a photocathode, a plate of Al alloy as an anode, and a U-shaped silicon rubber sheet as a spacer between the photocathode and anode to create a gap of 1 mm. The photocathode was back-illuminated with three UV light sources with wavelengths of 172 nm, 254 nm, and 265 nm. When the 172 nm UV source was used with a photocathode diameter of 15 mm, the stable discharge current reached more than 30 μA at 1500 V in Ar and more than 50 μA at 4000 V in air. The utilization of other UV sources with lower photon energies owns in lower quantum efficiencies and power densities showed stable and continuous discharge current, although the maximum current was limited. The current-voltage

characteristics suggested the occurrence of photoemission extraction and transport, then amplified via avalanche ionization. Optical emission spectroscopy showed emissions from Ar atoms, OH radicals, and N_2 molecules in Ar discharge and emissions from N_2 molecules in air discharge, besides the emission peaks of Xe I from UV light source. In addition, for analysis of reactive species production in gas discharge, UV absorbance spectroscopy measurement showed that air gas discharge induced by UV 172 nm produced reactive oxygen and nitrogen species including OH^-, NO_2^-, NO_3^-.

Acknowledgment

Foremost, I would like to express my deepest gratitude and thank to my supervisor, Prof. Akimitsu Hatta, for having faith in me and giving me an opportunity to join his laboratory. I appreciate all his thoughtful ideas, motivation and generously support in completion of my doctoral study. I am also thankful for an excellent example he has provided as a successful Professor and researcher.

I would like to express my sincere gratitude to Prof. Hiroshi Furuta for being very good Co-Supervisor during my study. His supports and comments allowed me to improve my work. I am also thankful to Prof. Hisao Makino, Prof. Chaoyang Li, and Prof. Mamoru Furuta, for their great advice and valuable feedback for my research.

My thanks and appreciation also go to Hatta-Furuta Laboratory members: Yajima-san (ORC Manufacturing Co., Ltd.) and Ikeda-san for their contributions in the beginning of this work; Adam, Nomura-san, Takino-san and Sawada-kun, for their assistance in laboratory as well as in daily life. I owe thanks also for my fellow PhD students, I-house members, and Indonesian members in Kochi for their friendship. Big appreciation to Ayat Al-Azab for her countless help both in sweet and bitter moment. Thank you for being really great friend. Special thanks also to my friends in Indonesia for always supporting me.

I am also very thankful to the staffs of International Relation Section and the staffs of Electronic and Photonic System Engineering department for their help and support. Also, I would like to thank to members of Rotary Yoneyama Shikoku district and Kochi Rotary Club for the financially and generously support. Especially my counselor, Takamura-san, and his family, thank you for taking care of me and making me feel the warmness of family.

Last but not least, I owe warm thanks to my parents, my brother and my big family for their love and encouragement during these three years.

Disclaimer

The study stated in this dissertation has not been previously submitted to meet the requirements for any award of degree. To author best knowledge, the dissertation contains no materials previously published or written by other person except where due reference is applied. The passages in some chapters in this dissertation have been quoted verbatim from the previous publications and works which were originally written by the author, listed as following:

Journal Papers:

1. Sukma W. Fitriani, S. Ikeda, M. Tani, H. Yajima, H. Furuta, A. Hatta, Hydrophilization of PTFE using DBD plasma of argon gas with water-ethanol vapor, *Mat. Chem. and Phys.*, 282 (2022) 125974, https://doi.org/10.1016/j.matchemphys.2022.125974

Conference Publications:

1. Sukma W. Fitriani, Y. Takino, H. Yajima, H. Furuta, and A. Hatta, *Surface Treatment for Hydrophilization of Polytetrafluoroethylene using Atmospheric-pressure Plasma by Argon Gas with Water-ethanol Vapor*, Proceeding of Eurodisplay 2022, September 21 – 23, 2022, Stuttgart-Germany

2. A. Hatta, Sukma W. Fitriani, H. Furuta, H. Yajima, *Treatment and Analysis of PTFE Surface using Atmospheric Pressure Water/Ethanol Mixture Vapor Plasma*, The 39th International Conference of Photopolymer Science and Technology, Materials and Process for Advanced Lithography, Nanotechnology and Photo technology (ICPST-39), June 28 – 29, 2022, Virtual conference

3. Sukma W. Fitriani, H. Yajima, H. Furuta, A. Hatta, *Plasma Treatment of Polytetrafluoroethylene in Nitrogen with Water/Ethanol Vapor Dielectric Barrier Discharge Plasma*, International Surfaces, Coatings, and Interfaces Conference (SURFCOAT Korea), May 26 – 28, 2021, Virtual Conference

4. Sukma W. Fitriani, H. Yajima, H. Furuta, A. Hatta, *Comparison between N_2 and Ar Gas with Water/Ethanol Vapor DBD Plasma for Surface Treatment of Polytetrafluoroethylene*, Proceeding of the 38th Symposium on Plasma Processing/The

33rd Symposium on Plasma for Materials (SPP-38/SPM-33), January 24 – 25, 2021, Virtual Conference

5. Sukma W. Fitriani, S. Ikeda, M. Tani, H. Yajima, H. Furuta, A. Hatta, *Hydrophilization of Polytetrafluoroethylene using Atmospheric Pressure Plasma o Argon Gas with Water and Ethanol Vapor*, Book of Abstract of 12th International Symposium on Advanced Plasma Science and its Applications for Nitrides/Nanomaterials 13th International Conference on Plasma-Nano Technology and Science (ISPlasma 2020/IC-PLANTS 2020), March 8 – 11, 2020, Nagoya-Japan

6. S. Ikeda, Sukma W. Fitriani, M. Tani, H. Yajima, H. Furuta, A. Hatta, *Modification of PTFE Surface by Atmospheric Pressure Plasma of Ar/ Water and Ethanol Vapor Mixture*, The 11th Asian Pacific Symposium on Plasma Technology (APSPT-11), December 11 – 14, 2019, Kanazawa-Japan

7. Sukma W. Fitriani, S. Ikeda, M. Tani, H. Yajima, H. Furuta, A. Hatta, *Modification of Polytetrafluoroethylene (PTFE) Surface by Atmospheric Pressure Plasma of Argon and Water-ethanol Vapor Mixture*, Nano-technology Symposium KUT, December 14, 2019, Kochi-Japan

The author originally wrote all the quoted sources.

Tables of contents

List of Figures

List of Tables

Abbreviation

AFM	: Atomic force microscope
APP	: Atmospheric pressure plasma
DBD	: Dielectric barrier discharge
DI water	: Deionized water
FWHM	: Full width half maximum
LMWOM	: Low molecular weight oxidized material
MS	: Mass spectroscopy
PTFE	: Polytetrafluoroethylene
ROS	: Reactive oxygen species
RNS	: Reactive nitrogen species
RONS	: Reactive oxygen and nitrogen species
UV	: Ultraviolet
WCA	: Water contact angle
XPS	: X-ray photoelectron spectroscopy

Chapter 1. Introduction

1.1. Fundamentals Theory

1.1.1. Plasma

Well-known as the 4th state of matter, plasma, is introduced by an American chemist, Irving Langmuir, for the first time in 1928. Plasma is composed of an equal number of free positive and free negative charges, also a different number of neutral molecules that are quasi-neutral in electrical. When sufficient energy in the form of an electric field, heat, or chemical reaction is supplied into a feeding gas it results in nearly fully ionized gas so-called hot plasma, or partially ionized gas so-called cold plasma. The degree of ionization of plasma α is described by the number of charged particles n_p $(=n_e)$ divided by the total number of particles N as follows: $\alpha = n_p/N$. [1]–[3].

Plasmas have been used in various applications including material processing, gas conversion, medical, agriculture, and light generation. Generally, for these applications, employed plasma is weakly ionized plasma with α in a range of 10^{-6} to 10^{-1} which is characterized by non-equilibrium, low temperature ranging from 300 K – 600 K, and low neutral gas density around 10^{13} to 10^{16} molecules/cm^{-3}. Non-equilibrium here refers to the different freedom degrees for each particle in plasma resulting in electrons temperature being around electron volts, while heavy particles temperature is around room temperature [4], [5]–[10].

Based on the operation pressure, plasma is distinguished into low-pressure plasma, atmospheric pressure plasma, and high-pressure plasma. Among them, atmospheric-pressure plasmas (APPs) non-equilibrium shows an excellent performance owing to their ability to give treatment to heat-sensitive materials and liquids. For example, in medical applications, the atmospheric pressure environment is necessary since biological materials cannot survive in vacuum conditions. This plasma is also known for its high reactivity owing plentiful production

of excited and ionized species. In addition, the absence of a vacuum system can reduce the cost of production. Hence, APP non-equilibrium has become popular not only for medical or agriculture applications but also for materials processing.

1.1.2. Plasma Generation

Gas discharge or plasma can be generated by applying a sufficient external field that caused a gas breakdown. The process of gas breakdown is initiated by free electrons from cosmic rays, radioactivity, and leftover charge. Then, they are accelerated by the electric field until gain enough energy to ionize the surrounding atoms which leads to electron avalanches production. Simply, two parallel planes as electrodes with gap separation d are connected to a DC power with a voltage V, thus, electric field, $E = V/d$, homogeneously generated (Figure 1. 1). In general, the primary electrons are found close to the cathode which drifts to the anode. During their mobility to the anode, they ionize the gas and generate electron avalanches [3], [4].
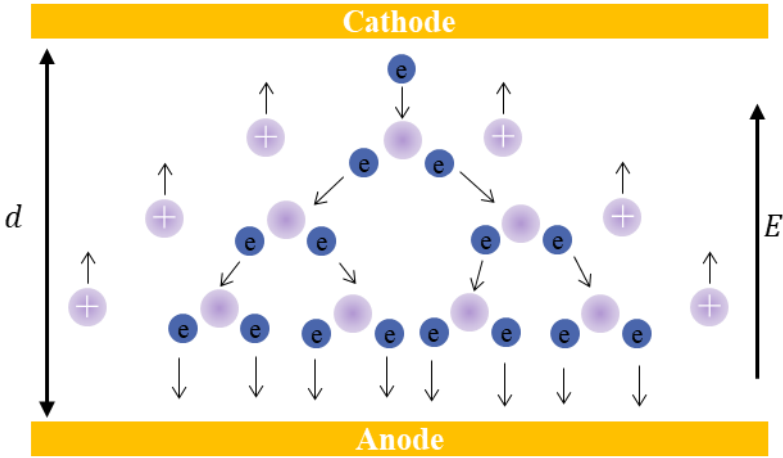
Figure 1. 1 Illustration of the Townsend breakdown

This process is considered the main feature of Townsend-breakdown. The self-sustained gas discharge can be obtained from electron avalanches that reached the anode successfully without the formation of space charge. Townsend ionization coefficient α describes the production of electrons per unit length through the electrical field, as follows:

$$\frac{dn_e}{dx} = \alpha n_e \text{ or } n_e(x) = n_{e0}\exp{(\alpha x)} \qquad (1. 1)$$

where n_{e0} is initial density of electron. The ionization rate coefficient $k_i(E/n_0)$ and electron

drift velocity v_d are related to the Townsend ionization coefficient as the equation below:

$$\alpha = \frac{v_i}{v_d} = \frac{1}{v_d} k_i\left(\frac{E}{n_0}\right) n_0 = \frac{1}{\mu_e} \frac{k_i(E/n_0)}{E/n_0} \tag{1.2}$$

The positive ions produced from the ionization process are moving to the cathode which

led to emitted electron generation, the so-called secondary electron. The probability of this

secondary electron emission is characterized by the Townsend coefficient γ. The gas

breakdown condition in the gap between electrodes can be described through the two Townsend

coefficients as follows:

$$\gamma[\exp(\alpha d) - 1] = 1, \qquad \alpha d = \ln\left(\frac{1}{\gamma} + 1\right) \tag{1.3}$$

Townsend coefficient α in equation 1. 2 can be rewritten in the form of parameters pressure p

as α/p and E/p. Then, based on this and equation 1. 3, a relation of the breakdown voltage

and electric field can be derived as the following expression:

$$\frac{\alpha}{p} = A \exp\left(\frac{B}{E/p}\right) \tag{1.4}$$

where A and B are the constant of each gas. From equation 1. 3 and 1. 4, the breakdown voltage

V_b and breakdown reduced electric field can be shown as function of parameters pd as follows:

$$V_b = \frac{B(pd)}{C + ln(pd)}, \qquad \frac{E}{p} = \frac{B}{C + ln(pd)} \tag{1.5}$$

Referred to equation 1. 5., Paschen curve describes the electrical breakdown voltage V_b versus

parameters pd as presented in Figure 1. 2. The minimum point of this curve shows the

minimum voltage required for gas breakdown indicating the easiest breakdown condition. On

the left side of V_b minimum, the electron avalanches at the anode without sufficient production

of ions. Thus, a significant increase in an electric field is necessary to boost the ionization

process. For the right side of V_b minimum, rising in breakdown voltage is required because the

reduction of the electric field in a larger electrode gap results in a lowering of electrons

acceleration. In addition, at higher pressure, electrons experience losing energy before being

3

able to ionize the surrounding atoms due to excessive collisions. Therefore, it must be redeemed by increasing of breakdown voltage.
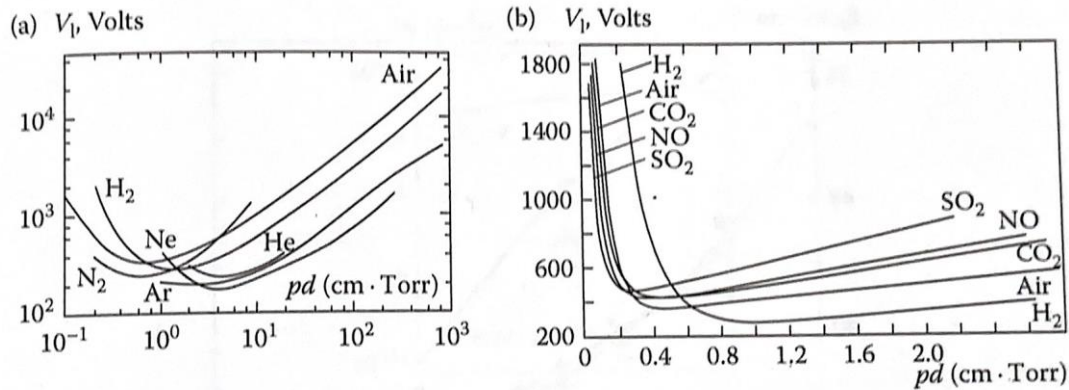
Figure 1. 2 Paschen curves for different gases (a) higher pressure range and (b) lower pressure range [3].

Typically, at atmospheric pressure, a homogeneous gas breakdown that includes the growth of independent electron avalanches occurs at $pd < 4000$ Torr. cm ($d < 5$ cm). In the case of a bigger electrode gap ($d > 6$ cm), the electron avalanches are not independent anymore because of the disturbance of an electrical field. As illustrated in Figure 1. 3, reduction of the electric field E/p is required to obtain breakdown voltage decreases logarithmically with parameters pd [3], [11]–[13].
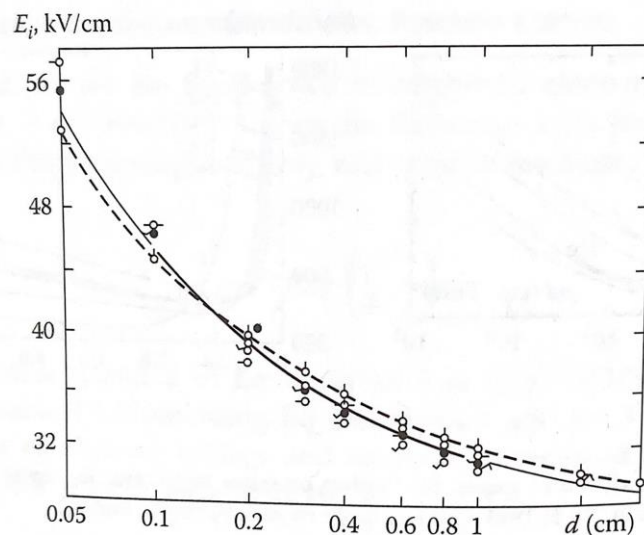
Figure 1. 3 Breakdown electric field in atmospheric air [3].
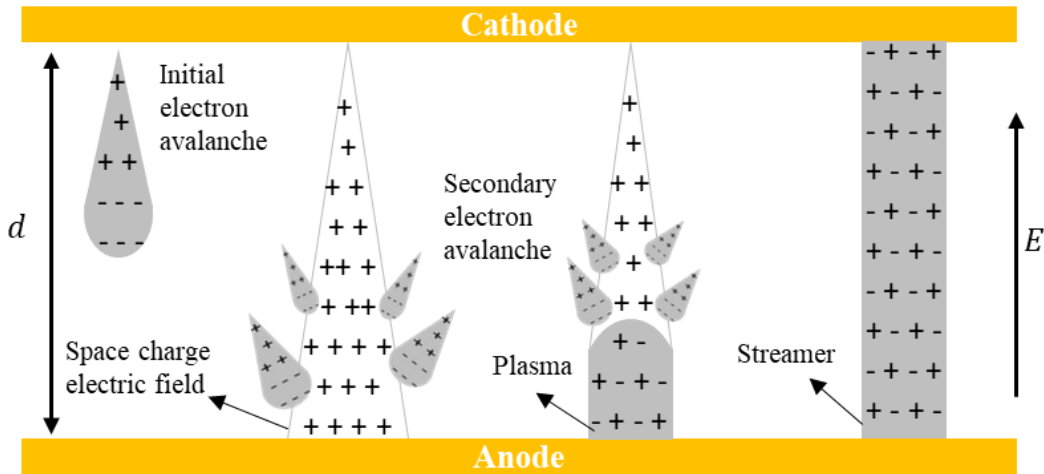
Figure 1. 4 Illustration of streamer gas breakdown formation.

Since the number of gas density becomes higher at elevated pressure, the density of collisions leads to ionization increases then changes the gas breakdown mechanism. Secondary electron avalanches are generated when an initial avalanche is forming a space charge which locally increases an applied electric field. In most cases, it is initiated by an electron detachment or photoionization. The rapid growth of this phenomenon builds a distinct plasma channel, known as a streamer (Figure 1. 4). The formation of streamers in air and other molecular gases at atmospheric pressure happens in nanoseconds time scale. Table 1. 1 presents the breakdown electric fields at high pressure for electronegative gases [1], [3]. Table 1. 1 presents the breakdown electric fields at high pressure for electronegative gases.

Table 1. 1 Electric fields sufficient for the Townsend breakdown of centimeters gaps at atmospheric pressure [3].

Gas	E/p (kV/cm)
Air	32
Ar	2.7
H_2	20
He	10
Ne	35
O_2	1.4

Meek criterion describes the gas breakdown through streamer formation as $exp(\alpha_{eff}.d)$ equal to 10^8, where α_{eff} is the effective value of first Townsend ionization coefficient. This expresses the minimum number of charge densities in the initial avalanches for gaining a significant field perturbation of space charge. Typically, this criterion is fulfilled at pd above 1000 Torr cm [1].
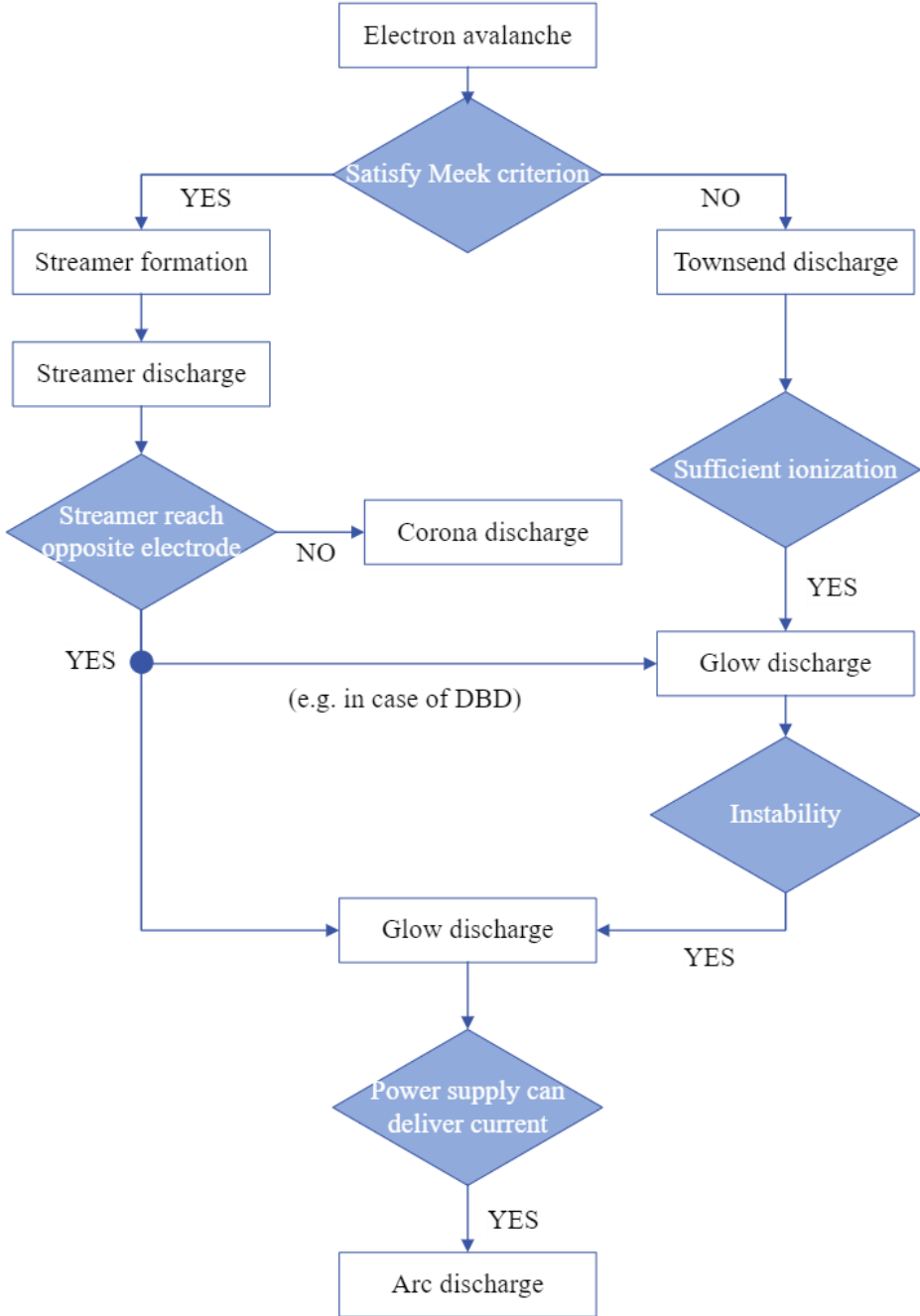
Figure 1. 5 Overview of the different transitions that occur in atmospheric pressure plasma discharges [1] .

Figure 1. 5 depicts an overview of typical discharge transitions in atmospheric pressure plasma. When the transition from differential gas breakdown mechanism happens, it often results in plasma instability. If the Meek criterion can be fulfilled, then diffuse and uniform gas discharge can be obtained. However, at high pressure, the gas discharge tends to be unstable which leads to the occurrence of the transition from a glow to a spark discharge on a time scale around 100 ns. The reason for unstable discharge is mostly due to the ionization and the recombination are not balanced induced by fluctuation in the temperature of gas and electron which leads to an extreme ionization process [1], [14]. An approach to prevent this happens is to make a limitation in discharge duration through short voltage pulses or using dielectric barrier discharge (DBD). DBD is described by placing a dielectric material in the discharge path. The dielectric materials such as glass, silicon rubber, ceramics, quartz, and Teflon. Depending on the electrode configuration and the gas, it required AC or pulsed high voltage ranging from 1 to 100 kV.

1.1.3. Photoelectric effect

A photoelectric effect is phenomenon when light with sufficient energy illuminates a material, resulting in the electron emission from the surface material. This is proposed in 1905 by Einstein in his explanation of the photo-electric effect. The electron can be ejected from the surface of material if the energy of the light (photon) $h\nu$ is higher than the potential barrier ϕ (depends on the material) of the electron to leave the surface and the balance energy is transformed to the kinetic energy E_k as expressed by following equation:

$$E_{kin_{\max}} = \frac{1}{2}m\vartheta_{\max}^2 = h\nu - \phi \qquad\qquad 1.\ 6$$
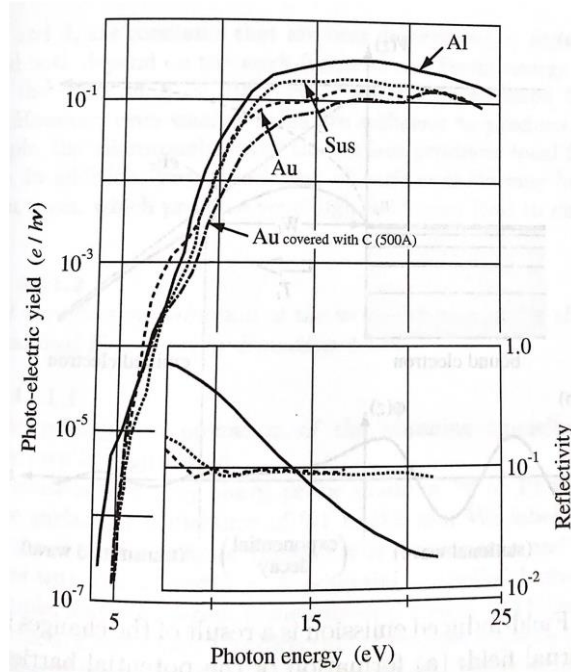
Figure 1. 6 Photo-emission yield for some metals as a function of photon energy [11].

Based on equation 1. 6., the kinetic energy of the electrons is affected by the photo energy rather than photon flux (number of photons). Thus, the electrons are emitted from the surface of the material if the photon energy $h\nu$ is bigger or at least the same as the potential barrier ϕ, $(h\nu - \phi = 0)$, regardless of the incident light intensity. The probability of a single photon inducing electron emissions called photoelectric yield, for some metals, is shown in Figure 1. 5 [11]. Photoemission is a promising candidate for supplying free electrons which are required in obtaining a stable discharge at high pressure.

1.2. Motivation and research issue

In recent years, APPs have been receiving massive popularity in various fields, including surface materials processing, medical, gas conversion, agriculture, and aerospace due to higher production of reactive species in less vacuum conditions [15]–[20]. However, in comparison with low-pressure plasma, generating uniform and stable plasma in atmospheric pressure is still facing some issues. At elevated pressure, gas discharge is easily to be unstable and non-uniform because of the transition from glow discharge to arc or spark discharge happens [14]. Thus, generating stable and uniform atmospheric pressure plasma is required

8

special methods, such as the utilization of special electrode arrangements and specific excitation methods.

DBD plasma is one of the alternative plasma generations which prevent the formation of spark or arc discharge in atmospheric pressure conditions which typically occurs on a time scale of ~ 100 ns [1]. By placing dielectric materials in the discharge gap, the limitations of the discharge duration can be achieved leading to stable discharge generation. Furthermore, since it does not require advanced pulse power supplies and equilibrium conditions, DBD plasma can be operated easily even under atmospheric pressure environments. Due to this, DBD plasma becomes a cost-effective and harmless tool for surface materials treatment, especially polymer which can be treated at high-temperature conditions.

Polytetrafluoroethylene (PTFE) has several useful properties, such as chemical inertness, a non-wetting surface, and a low coefficient of friction [21]–[23]. However, PTFE exhibits poor adhesion, because of which it does not stick adequately onto other materials. This property needs to be improved for an appropriate adhesion of various coatings, for example at gluing, printing, or deposition with specific functionality. Application of DBD for PTFE surface treatment using various electrode arrangement and various gas discharge have been reported in several works [24]–[28]. However, a lot of challenges still need to be solved.

Low-temperature air plasma generated in atmospheric pressure has been shown a positive result in agriculture and medical applications. It was reported that air plasma is beneficial for seed germination, drug delivery, tissue engineering, and cancer treatment [9], [16], [17], [29], [30], [31]. This plasma produces reactive oxygen species (ROS) consisting of ozone, hydroxide radicals, and nitrogen species (RNS) which are responsible for the killing effect and healing effect. It occurs through the interaction of plasma with biological materials producing free electrons, and reactive species such as O and NO.

Moreover, the selection of air as a working gas in plasma generation brings out advantages owing to simple design and low cost in operational compared to the other gasses, for example, H_2, Ar, and N_2. However, the stability and uniformity of air plasma need to be improved to ensure and widen its utilization in industries. Hence, the development of atmospheric pressure plasma induced by photoemission could be one possible way to obtain stable air plasma for medical and agricultural applications.

1.3. Research objectives

The main objective of this dissertation is to utilize atmospheric pressure plasma for PTFE functionalization and to develop novel atmospheric pressure gas discharge induced by photoemission for medical and agriculture application. The detail objectives from this research are listed below:

- Improving the wettability of PTFE using dielectric barrier discharge plasma of Ar with water-ethanol and N_2 with water-ethanol.

- Studying the mechanism of dielectric barrier discharge plasma of Ar with water-ethanol and N_2 with water-ethanol for PTFE surface functionalization.

- Generating a stable atmospheric pressure gas discharge induced by photoemission using argon and air as well as studying the mechanism of it.

1.4. Thesis Outline

The thesis is organized as follows:

Chapter 1 presents an introduction of the work including the fundamentals theory, the research motivations and issues, and the research objectives. Furthermore, the organization of the thesis is presented also.

Chapter 2 presents the dielectric barrier discharge plasma of gas mixture with water and ethanol vapor for surface modification of PTFE. Ethanol concentration and plasma treatment duration variation were performed in Ar and N_2 as carrier gas. In addition, plasma mass

spectroscopy and stability examination were performed. The introduction, objectives, experimental methods, and results are described. Lastly, discussions and conclusions are drawn based on the experimental results.

Chapter 3 presents the surface analysis of PTFE after plasma treatment. The analysis includes morphology using AFM and chemical analysis using XPS. The introduction, objectives, experimental methods, and results are described. Lastly, discussions and conclusions are drawn based on the experimental results.

Chapter 4 presents the generation of atmospheric pressure plasma induced by photoemission. Photoemission was produced by back-irradiation of electrode gold thin film with three different kinds of UV sources. The analysis was carried out by measuring the current-voltage relationship. The introduction, objectives, experimental methods, and results are described. In the end, discussions and conclusions are drawn based on the experimental results.

Chapter 5 is a summary of this dissertation drawn from each chapter.

Chapter 2. DBD plasma of gaseous with water-ethanol vapor for surface modification of PTFE

2.1. Introduction

Polytetrafluoroethylene (PTFE) has several useful properties, such as chemical inertness, a non-wetting surface, and a low coefficient of friction [21]. However, PTFE exhibits poor adhesion, because of which it does not stick adequately onto other materials. This property needs to be improved for an appropriate adhesion of various coatings, for example at gluing, printing, or deposition with specific functionality. Plasma treatment can selectively modify only the surface of the polymer without changing its bulk properties, and does not produce harmful by-products [32], [33]. Several studies have investigated the plasma treatment of PTFE using different types of plasma (e.g., low-pressure and atmospheric-pressure plasma) and gasses (e.g., He, O_2, N_2, and Ar), which indicated that the treatment can increase surface wettability [27], [34], [35]. Among these plasma treatment methods, atmospheric-pressure plasma has a huge advantage in the industrial field because it does not require a vacuum system and enables rapid material processing.

In a related study of hydrophilization of PTFE by plasma treatment, Shibahara et al. investigated a series of liquids (water, methanol, ethanol, and acetone) as vapor sources in atmospheric-pressure plasma for PTFE modification [36]. They reported that the addition of 1% ethanol vapor in helium gas results in a significant reduction of water contact angle from 110° to 30° after 30 minutes of treatment. Nevertheless, the hydrophilization was still limited and required rather long treatment. Furthermore, Hai et al. [37] successfully improved the wettability of PTFE using a low-temperature plasma of argon bubbled in a water–ammonia solution. The water contact angle (WCA) of the PTFE film decreased from 118° to 4° after 20 min of treatment. The mixture of water and ammonia appears to be effective for improving the wettability of PTFE surfaces. However, ammonia is not suitable for atmospheric-pressure

plasma operated in open air because it is harmful to the environment. Consequently, plasmas of water mixed with another liquid are a potential option for improving the wettability of PTFE.

The hydrophilic effects after plasma treatment may restore the polymer surface wettability to its original state because of the molecular motion or weak boundary layers; this process is described as degradation/recovery [38]–[41]. Nakamatsu et al. [40] reported that plasma-modified PTFE is strongly affected by the storage conditions, including the environment (solution and air) and temperature. Deynse et al. showed that, polymer modification using a dielectric barrier discharge (DBD) plasma of N_2 mixed with ethanol vapor can improve the surface wettability, due to polymerization of the nitrogen- and oxygen-containing groups on the polymer surface. In addition, this type of plasma polymerization can suppress the degradation effects of the plasma treatment [42], [43]. Another study reported that oxygen loss occurs on the plasma-treated polymer upon washing with water [44]. Hence, the stability of the plasma-modified surface is an important issue for extending the application of PTFE.

Mass spectroscopy is a possible plasma diagnostic method than can measure a wide range of plasma species, for example, positive ions, negative ions and neutral. Mass spectroscopy of atmospheric-pressure plasma has been performed to obtain a better understanding of the plasma treatment process [45]–[47]. Beck et al. [45] performed ions mass spectrum measurement during polymer treatment using atmospheric-pressure helium plasma. Mass spectroscopy also can be used to predict the final surface state and coating contamination to propose the mechanism of plasma treatment [48].

2.2. Objectives

This study aims to improve the surface wettability of PTFE using DBD plasma of Ar or N_2 mixture with water-ethanol vapor effectively and efficiently. The effect of ethanol concentration and plasma treatment duration on the wettability will be investigated. Prior to

that, quadrupole mass analysis will be utilized to measure the plasma species as well as measure the current-voltage characteristic. In addition, the stability of plasma-treated surface will be evaluated also by immersing the plasma-treated PTFE in deionized water (DI water).

2.3. Experimental and Methods

Figure 2. 1 shows the experimental setup used for PTFE plasma treatment. Atmospheric-pressure plasma was generated by DBD using a pair of copper electrodes (10 mm × 10 mm) placed on the external surface of parallel glass plates (40 mm × 50 mm × 1 mm). Ethanol (Nacalai Tesque Inc., purity 99.8%) was dissolved in DI water at various concentrations ranging from 0% to 100%. Then, 50 g of solution was added to a bubbling bottle placed in a water bath maintained at 20°C. Ar or N_2 gas was bubbled into the water-ethanol solution at a flow rate of 500 sccm, and the gas mixture (Ar/ N_2 and water-ethanol vapor) was introduced into the discharge cell between the parallel plates. A high-voltage sinusoidal wave was applied to one of the electrodes at a peak-to-peak voltage 10 kV for Ar and 15 kV for N_2 and frequency of 25 kHz; the other electrode was grounded.
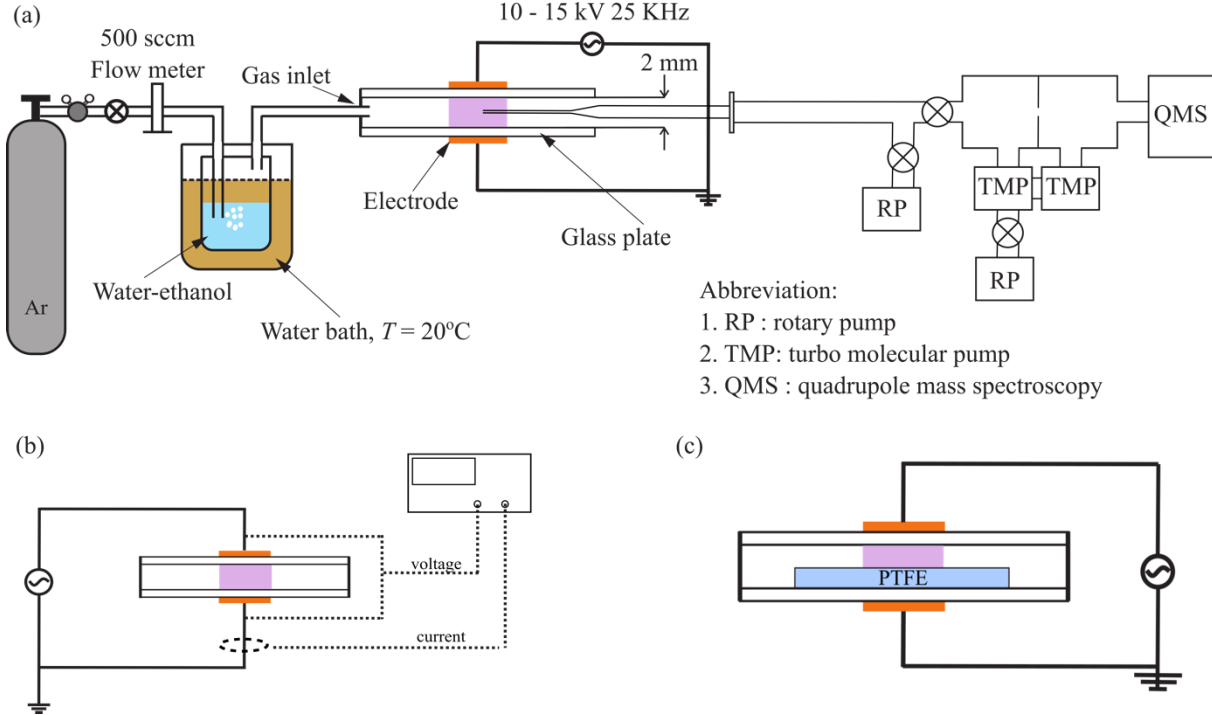
Figure 2. 1 Experimental setup for plasma treatment using gas with water-ethanol vapor (a) gas analysis measurement (b) current discharge measurement (c) specimen plasma treatment

A quadrupole mass analyzer (Anelva M-200QA-M) was employed to analyze the gas composition in the plasma. A Pyrex glass capillary with an inner diameter of 35 μm and outer diameter of 200 μm was inserted into the center of the discharge cell, as shown in Figure 2. 1 (a). The glass capillary was evacuated using an oil rotary pump, and the sampled gas was further introduced into a high-vacuum chamber equipped with the quadrupole mass analyzer head and a differential pumping system consisting of two turbo molecular pumps. The quadrupole mass analyzer was operated to record in an m/z range from 0 to 50 amu with a secondary electron multiplier of 1200 V for ion current detection, an emission current of 50 μA, and an electron energy of 100 eV for ionization of neutral species. Owing to the small conductance of the glass capillary, the ionic species in the plasma could not be detected directly. The mass spectra sampled through the glass capillary only included those of the stable and neutral species, then some fragmented ionized species by the quadrupole mass analyzer were detected. Because the quadrupole mass analyzer also detected the residual gas in the high-vacuum chamber, the gas spectrum was evaluated by the difference between the collected data and the detected residual gas.

The discharge voltage and current were measured using high voltage probe (Tektronix, P6015A) and current monitor (Pearson 2877), respectively. The electrical signals were monitored using digital oscilloscope (Iwatsu, DS-5012), as shown in Figure 2.1 (b).

The plasma treatment was performed on a PTFE sheet (Flon Industry Co. Ltd.) with a thickness of 1 mm cut into a 30 mm × 30 mm square. The PTFE sheet was placed on the lower glass plate, as shown in Figure 2. 1(c), leaving a 1 mm gap from the upper glass plate. Before the plasma treatment, the specimens were ultrasonically cleaned for 5 min in each of three different liquids: first acetone, then DI water, and finally ethanol. The plasma was generated over a profile area of 10 mm × 10 mm square corresponding to the electrodes, which was smaller than the specimen size to avoid non-uniform discharge at the edge of the specimen. The

plasma treatment was conducted in an open atmosphere for operation times varying from 1 to 20 s.

The wettability of the specimen was characterized by measuring the static WCA at three different positions in the plasma-treated area. A 1 μL water droplet was dropped on each position. After 30 s, an image of the droplet was captured for the WCA measurement using a digital-microscope (VH-5500, KEYENCE Co. Ltd.). The stability of the plasma-treated PTFE surface was examined by immersing the specimen in DI water for 3 min after the plasma treatment. The sample was then kept at room temperature with humidity of 30%-40% for 60 min before surface characterization.

2.4. Results and Discussion

2.4.1. Plasma discharge current and profile

Figure 2. 2. depicts typical discharge voltage and current of DBD plasma of Ar with water-ethanol and N_2 with water-ethanol at the operating voltage peak-to-peak of 10 kV and 15 kV, respectively. For determining of the discharge current, the displacement current (condition in the absence of the discharge but with the applied voltage) was subtracted from the total current measured. The typical discharge current shows two single peaks per period associated with the positive and negative parts of the voltage cycle. From the obtained waveform above, the input power was calculated using equation below:

$$P_{in} = \frac{\int_0^T V(t) \times I_D(t) dt}{T}$$

Where T is the time for half a period (20 μs), V is the applied voltage, and I_D is the discharge current. Both V and I_D are time dependent. The power density is 1.2 W/cm^2 for Ar as gas carrier and 2.2 W/cm^2 for N_2 as gas carrier.
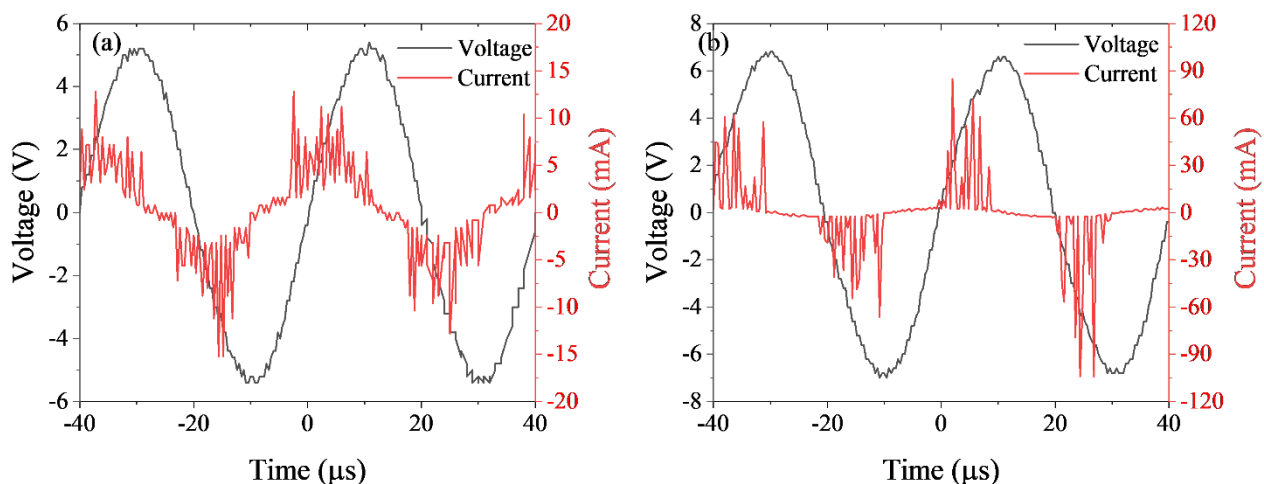
Figure 2. 2 Discharge current of DBD plasma in different gas discharge (a) Ar with water-ethanol and (b) N$_2$ with water-ethanol
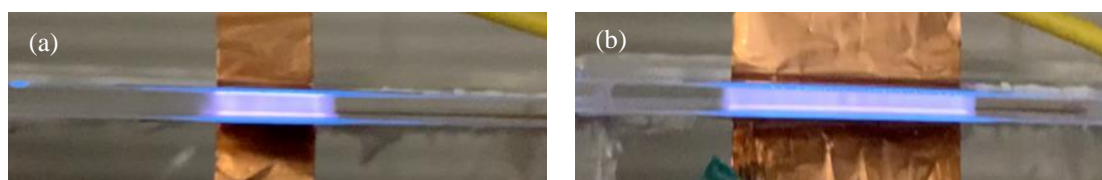
Figure 2. 3 DBD plasma profile of Ar with water-5% ethanol with different size area of electrode (a) 100 mm^2 and (b) 300 mm^2

In general, DBD plasma is sustained through filament discharge which occurs between two electrodes (one or all is covered by dielectric materials). In the current study, the DBD plasma profile is depicted in Figure 2. 3, although the filament was not observed clearly. The DBD plasma was generated using different sizes of the electrode to examine the homogeneity of the plasma. The plasma exhibited almost a similar profile even though the electrode size was extended up to 300 mm^2. In section 2.4.3., the homogeneity of plasma will be evaluated by measuring the water contact angle on the plasma-treated PTFE surface.

2.4.2. Gas Analysis

Figure 2. 4 depicts the mass spectrum of gaseous species in the discharge cell of Ar with water-ethanol at different ethanol concentrations with and without plasma operation. For all ethanol concentrations, when the plasma was OFF, there were two dominant peaks at $m/z = 40$ and $m/z = 20$, which correspond to monovalent Ar ions ($40Ar^+$) and divalent Ar ions ($40Ar^{2+}$).

In addition, trivalent Ar ions at $m/z = 13.3$ (Ar^{3+}) and Ar isotopes at $m/z = 36$ ($36Ar^+$) were present with lower intensities. These peak intensities for Ar were almost constant regardless of the ethanol concentration because the saturated vapor pressures of water and ethanol were two orders of magnitude lower than the atmospheric pressure of Ar.
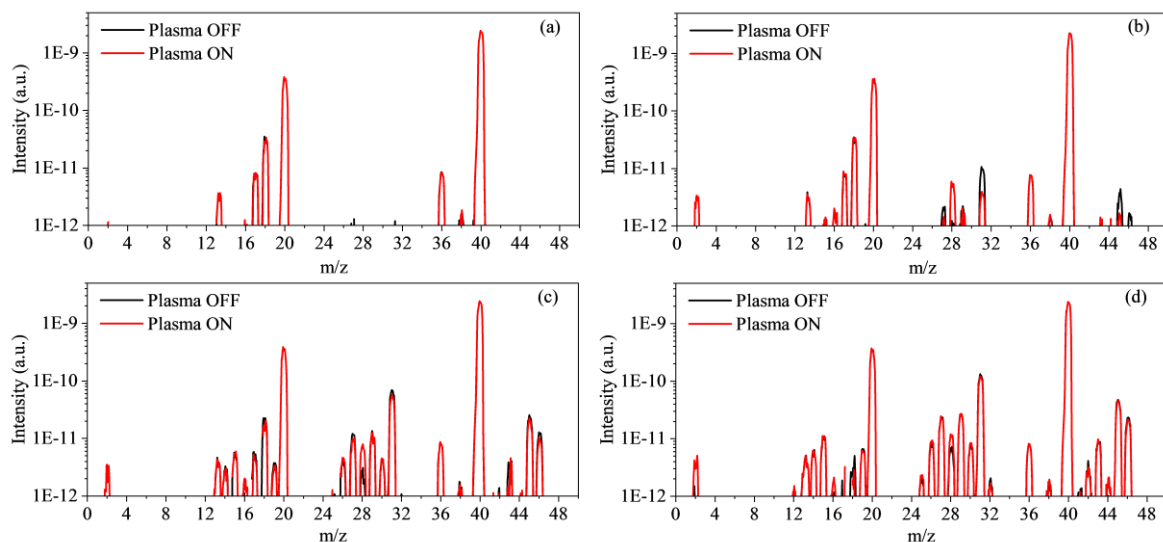
Figure 2. 4 QMS of Ar with water-ethanol with various ethanol concentrations: (a) 0%, (b) 5%, (c) 50%, and (d) 100%.

In the mass spectrum of pure water vapor in Ar (Figure 2. 4 (a)), fragmented ions from water molecules at $m/z = 17$ (OH^+) and water ions at $m/z = 18$ (H_2O^+) were significant in addition to the Ar peaks when the plasma was OFF. When the ethanol concentration was 5% (Figure 2(b)), additional peaks appeared at $m/z = 26, 27, 29, 31, 45,$ and 46. The highest peak for ethanol was confirmed at $m/z = 31$, which agrees with the NIST data [49]. When the ethanol concentration was increased to 50% and 100% (Figure 2. 4 (c) and (d), respectively), the peak intensities of fragmented ions from ethanol increased in a similar manner, and some additional small peaks were detected at $m/z = 14, 15, 19, 25, 26, 28, 42, 43,$ and 44, which were also fragmented from ethanol. The fragmented ethanol peaks were assumed to be hydrocarbons (C_2H_n and C_3H_n). On the other hand, the peak intensities for water at $m/z = 17$ and 18 decreased with increasing the ethanol concentration.

When the plasma was turned ON, the measured peak intensities for Ar at $m/z = 40$, 20, 13.3, and 36 decreased to 75 % in comparison with those when plasma was OFF (the original spectra with lower intensities are not presented in Figure 2. 4). The decrease in peak intensities when the plasma was turned ON could be due to gas heating in the discharge cell. The gas temperature increased owing to heating by the discharge plasma while the pressure was balanced with the atmospheric pressure, resulting in a decrease in the number density of gas molecules. Assuming that all the peak intensities were affected by the gas temperature in the same manner (to compare the gas composition ratio with and without plasma), the spectra when the plasma was ON expanded to compensate for the effect of gas heating and to match the Ar peak intensity at $m/z = 40$. After calibrating for the different intensities, most of the peaks overlap between the plasma ON and OFF states, with some exceptions that are described below.

For pure water vapor ion Ar (0% ethanol, Figure 2. 4 (a)), the spectra completely overlapped when the plasma was turned ON and OFF. This indicates that water vapor does not induce any chemical products, even if it can be decomposed in the plasma. For pure ethanol vapor in Ar (100 % ethanol, Figure 2(d)), when the plasma was turned ON, the peak intensity at $m/z = 28$ (assigned to CO) clearly increased, and small peaks appeared at $m/z = 2$ and $m/z = 16$ (assigned to H_2 and CH_4, respectively). The characteristic peak for ethanol at $m/z = 31$ decreased slightly by 9.8 %. This indicates that, in the plasma, ethanol molecules are decomposed, and H_2, CH_4, and CO molecules are produced. When the ethanol concentration decreased to 50% and 5% with increasing water concentration (Figure 2. 4 (c) and 2. 4 (b), respectively), the decrease in peak intensity at $m/z = 31$ and increase in peak intensity at $m/z = 28$ became more significant. The peak intensity for the H_2 molecule was almost constant, even when the ethanol concentration decreased from 100% to 5%. In addition, because the quadrupole mass analysis detected numerous ionized hydrocarbon fragments from ethanol, it

was expected that the concentration of hydrocarbon species in the plasma would also increase when the ethanol concentration increased.

The experimental results indicated the presence of H_2, CH_4, and CO produced from ethanol in the plasma. Ethanol decomposition follows the reaction below:

$$C_2H_5OH \rightarrow H_2 + CO + CH_4 \qquad \text{(R.1.)}$$

If H_2, CH_4, and CO were directly produced from ethanol (as indicated in (R.1.)), the production of these molecules would be proportional to the ethanol concentration. However, the results indicates that both the decomposition of ethanol and the production of H_2, CH_4, and CO were not enhanced by increasing the ethanol concentration. The reaction was nearly saturated at a low ethanol concentration of 5%, yielding small changes when the ethanol concentration was increased.

It has been mentioned in related studies that water vapor plays an important role of ethanol decomposition in the DBD plasma [50], [51]. The addition of water is favorable in the ethanol decomposition through the following reaction [6]:

$$C_2H_5OH + H_2O \rightarrow 4H_2 + 2CO \qquad \text{(R.2.)}$$

Wang et. al [50] suggested that the enhancement of ethanol conversion reaction by increasing water/ethanol mole ratio (decreasing ethanol concentration) might be due to oxygen and hydroxyl radicals from water molecules, which are more active in transferring energy and colliding with ethanol molecules to promote ethanol decomposition. At a low concentration of 5% ethanol, the ethanol peak intensity at $m/z = 31$ decreased by 70 % when the plasma was turned ON. On the other hand, the peak m/z 31 reduced by 43% and 38% for ethanol concentrations of 50% and 100%, respectively. Therefore, it was quantitatively demonstrated that water vapor enhanced the decomposition of ethanol in plasma. Notably, the production of H_2 remained almost unchanged, even when the ethanol was diluted with water to a low concentration of 5%.
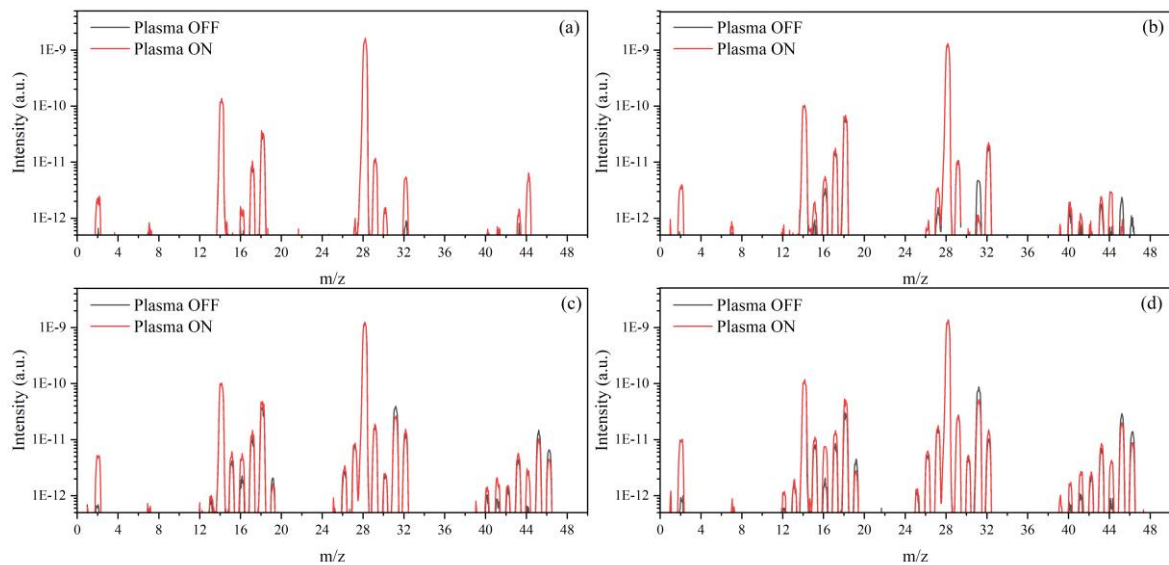
Figure 2. 5 QMS of N_2 with water-ethanol with various ethanol concentrations: (a) 0%, (b) 5%, (c) 50%, and (d) 100%.

Figure 2. 5 depicts the mass spectrum of gaseous species in the discharge cell of N_2 with water-ethanol at different ethanol concentrations with and without plasma operation. For all ethanol concentrations, when the plasma was OFF, there were two dominant peaks at $m/z = 14$ and $m/z = 28$, which correspond to the existence of N_2. In addition, another peak at $m/z = 29$ was present with lower intensities. These peaks intensity for N_2 were almost constant regardless of the ethanol concentration because the saturated vapor pressures of water and ethanol were two orders of magnitude lower than the atmospheric pressure of N_2.

In the mass spectrum of pure water vapor in N_2 (Figure 2. 5 (a)), fragmented ions from water molecules at $m/z = 17$ (OH^+) and water ions at $m/z = 18$ (H_2O^+) were significant in addition to the N_2 peaks when the plasma was OFF. In addition, small peak at $m/z = 32$ and 16 were detected as fragmentation of oxygen which possibly from atmosphere. When the ethanol concentration was 5% (Figure 2.5 (b)), additional peaks appeared at $m/z = 15, 27, 31, 40, 41, 42, 43, 45,$ and 46. The highest peak for ethanol was confirmed at $m/z = 31$, which agrees with the NIST data [26]. When the ethanol concentration was increased to 50% and 100% (Figure2. 5 (c) and (d), respectively), the peak intensities of fragmented ions from ethanol increased in a similar manner, and some additional small peaks were detected at $m/z = 13, 19, 25, 26, 30,$ and

21

44, which were also fragmented from ethanol. The fragmented ethanol peaks were assumed to be hydrocarbons (C_2H_n and C_3H_n). On the other hand, the peak intensities for water ($m/z = 17$ and 18) and oxygen ($m/z = 16$ and 32) decreased with increasing the ethanol concentration.

When the plasma was turned ON, the measured peak intensities for N_2 at $m/z = 14$, 28 and 29 decreased to 80 % in comparison with those when plasma was OFF (the original spectra with lower intensities are not presented in Figure 2. 5). The decrease in peak intensities when the plasma was turned ON could be due to gas heating in the discharge cell as explained in Ar case. After calibrating for the different intensities based on the N_2 peak intensity at $m/z = 28$, most of the peaks overlap between the plasma ON and OFF states, with some exceptions that are described below.

For pure water vapor in N_2 (0% ethanol, Figure 2. 5 (a)), new peaks were found at $m/z = 2$, 30, and 44 which corresponded to the existence of H_2, NO and N_2O, respectively. Furthermore, the peak intensity of oxygen at $m/z = 16$ and 32 increased drastically. For pure ethanol vapor in N_2 (100 % ethanol, Figure 2. 5 (d)), when the plasma was turned ON, the peak intensity of water and oxygen increased as well as peaks at $m/z = 2$, 12, 40, 41, 44. The detection of both peak at m/z = 12 and 44 can be assigned as CO_2. In addition, the characteristic peak for ethanol at $m/z = 31$ decreased slightly. When the ethanol concentration decreased to 50% and 5% with increasing water concentration (Figure 2. 5 (c) and 2. 5 (b), respectively), the decrease in peak intensity at $m/z = 31$ became more significant. The peak intensity at $m/z = 2$ and $m/z = 44$ were almost constant, even when the ethanol concentration decreased from 100% to 5%. These results indicate that, chemical reaction was occurred when plasma ON, most probably decomposition of ethanol and its reaction with N_2. As a result, H_2, CH_4, CO_2, NO, and N_2O molecules were produced.

2.4.3. PTFE Wettability evaluation

The wettability of the PTFE surface was evaluated by static WCA measurements before and after plasma treatment and after immersion in DI water. A 10 μL of DI water was dropped on the PTFE surface then followed by capturing an image. The measured contact angle was defined by the angle of the water droplet to the PTFE surface θ as shown in Figure 2. 6. Improvement of wettability was achieved after plasma treatment as the reduction of WCA.
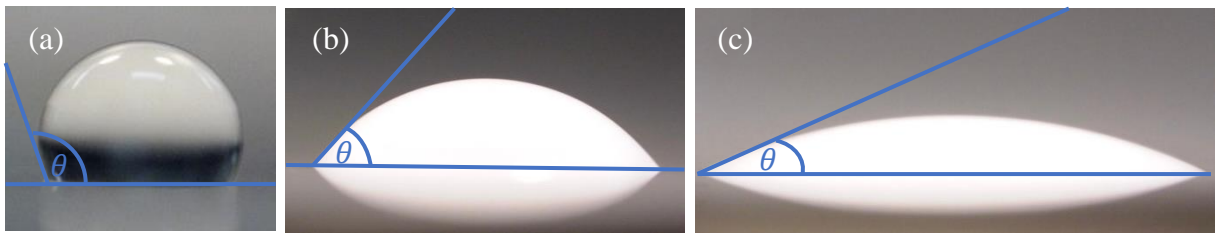
Figure 2. 6 WCA of (a) untreated PTFE and plasma-treated PTFE using (b) Ar with water– 5% ethanol (c) N_2 with water–5% ethanol.

Figure 2. 7 shows the water droplets on the PTFE in size of 70 mm x 20 mm after plasma treatment of Ar with water-5% ethanol for 10 s. The water droplets were placed in seven positions along the specimen which had a similar profile of water droplets. It indicates that generated DBD plasma was homogeneous even though the electrode size was extended to 50 mm x 10 mm.

Figure 2. 7 Water droplets on the plasma-treated PTFE in size of 70 mm x 20 mm to examine the homogeneity of plasma treatment.

The detail effect of plasma treatment on the PTFE wettability is explained in the following sub-section which is divided by Ar with water-ethanol part and N_2 with water-ethanol part.

23

2.4.3.1 Ar with water-ethanol

Figure 2. 8 shows the WCA of PTFE treated by plasma for 5 s as a function of the ethanol concentration, which varied from 0% to 100%. The WCA of the original PTFE surface was 115°. The WCA decreased to 77° after plasma treatment for 5 s, even with 0% ethanol (pure water vapor) in Ar. At an ethanol concentration of 1% to 2%, the improvement in the WCA was almost the same as that for pure water.

Figure 2. 8 WCA of the PTFE after 10 s treatment with plasma of Ar with water-ethanol as a function of ethanol concentration.

When the ethanol concentration was increased to 3%, the WCA decreased significantly to 50°. For ethanol concentrations between 3% and 9%, the WCA remained almost constant at 50°, which is less than half that of the original PTFE surface. When the ethanol concentration was increased to 12%, the WCA increased to more than 65°. Then, as the ethanol concentration was further increased to 40%, 60%, and 100%, the WCAs were 72°, 70°, and 55°, respectively. Therefore, the wettability of the PTFE surface was remarkably improved by the plasma treatment of ethanol/water vapor in Ar at small ethanol concentrations (3%–9%) in water.

The evolution of the WCA as a function of the plasma treatment time is shown in Figure 2. 9 (a). The plasma treatment time was varied from 1 to 20 s at small ethanol concentrations of 3%, 5%, and 9%. Even with the shortest plasma treatment (1 s), the WCA clearly decreased

from 115° (untreated PTFE) to approximately 82°. At all the examined ethanol concentrations, the WCA decreased with increasing plasma treatment time until 10 s and then leveled off below 20°.

Figure 2. 9 WCA of PTFE after plasma treatment of Ar with water-ethanol as a function of treatment time (a) with low ethanol concentration (b) comparison before and after immersion in DI water

The stability of the plasma-induced wettability of the PTFE surface was examined by immersing the specimen in DI water. Figure 2. 9 (b) shows a comparison of the WCA of PTFE plasma-treated with 5% ethanol for various treatment times before and after immersion in DI water. For the specimens treated for 1 and 5 s (where the WCA continued to decrease with increasing treatment time), there was no significant degradation of the WCA due to immersion in DI water. For the specimens treated for 10, 15, and 20 s (where the wettability was well improved by the plasma treatment, and the WCA was almost saturated at approximately 20°), the WCA increased to 50° after immersion. After the short-duration plasma treatment, the wettability did not improve adequately, but it remained stable after immersion in DI water. After a sufficient duration of plasma treatment (more than 10 s), the achieved wettability was easily degraded by immersion in DI water. It appears that there is a limitation in the stable modification of the PTFE surface induced by plasma treatment at WCA of approximately 50°.

2.4.3.2 N$_2$ with water-ethanol

Figure 2. 10 shows alteration of PTFE wettability after 10 s exposed to plasma with different ethanol concentrations diluted in N$_2$. WCA angle as received PTFE, 115°, decreased to around 95 ° in case of N$_2$ mixture with water vapor (0% ethanol). On the other hand, a significant drop of WCA to 30° was observed by adding 3 % of ethanol as a working gas. Furthermore, as ethanol concentration increased to 5%, 9%, 50% and 100%, the wettability of PTFE experienced the optimum improvement, resulting in a WCA of 12°. It is suggested that the addition of ethanol could improve the wettability, yet it was not strongly affected by ethanol concentration.
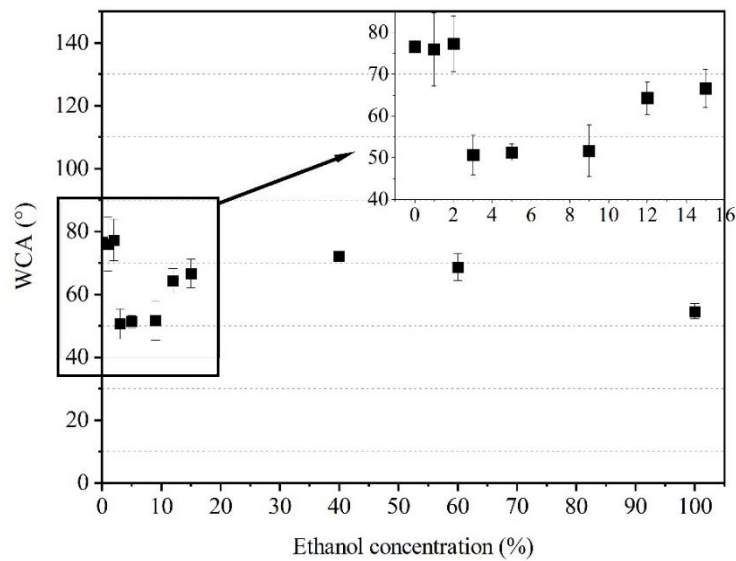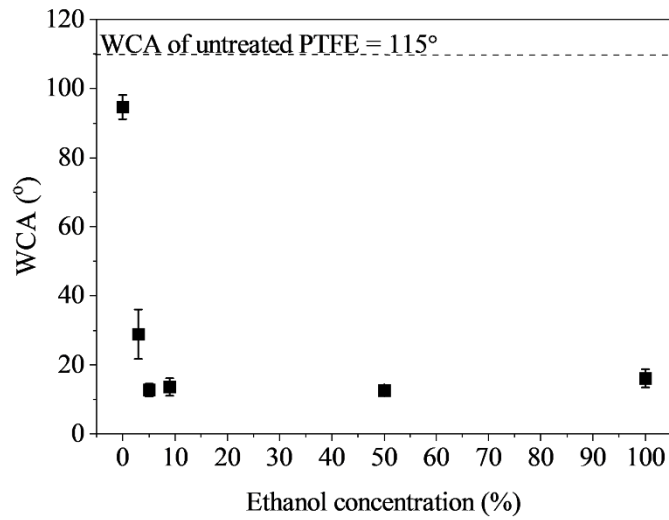

Figure 2. 10 WCA of the PTFE after 10 s treatment with plasma of N$_2$ with water-ethanol as a function of ethanol concentration
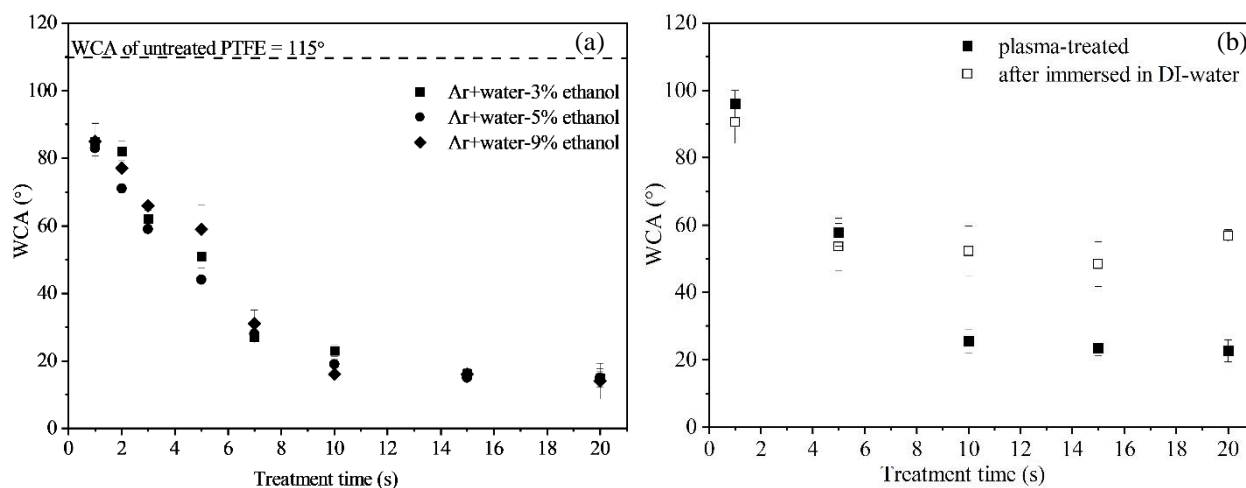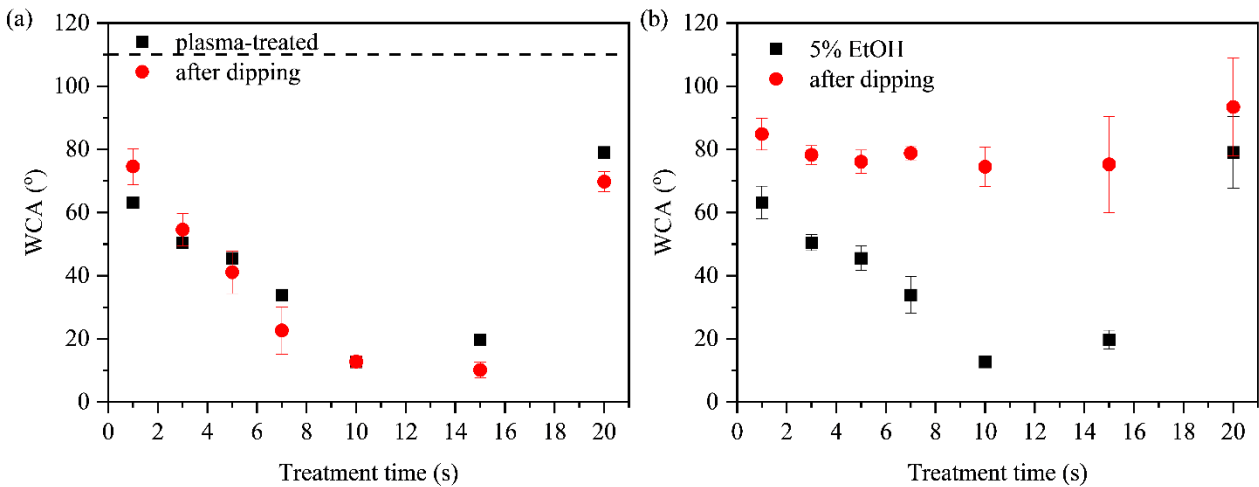

Figure 2. 11 WCA of the PTFE after plasma treatment of N$_2$ with water-ethanol as a function of treatment time (a) with low ethanol concentration (b) comparison before and after immersion in DI water

Figure 2. 11 (a) depicts the evolution of the WCA as a function of plasma treatment time which varied from 1 s until 20 s using N_2 with water-ethanol as gas discharge. After being exposed to plasma for 1 second, the wettability of PTFE was improved from hydrophobic to hydrophilic with a WCA of around 60°. With increasing treatment time, the WCA kept decreasing to around 10° for 15 seconds of treatment. However, plasma treatment for more than 15 seconds resulted in wettability recovery. The WCA was increased drastically up to 70°. As mentioned in section 2.4.1 that N_2 plasma has a higher power density than Ar, this could lead to a rising in the surface temperature as treatment time increased. Then, it possibly influenced the plasma treatment mechanism resulting in hydrophobic recovery. Furthermore, WCA degradation also occurred after immersing plasma-treated PTFE in DI water as shown in Figure 2. 11 (b). In comparison with Ar as a gas carrier, the degradation of N_2 is more severe. In all treatment time, WCA degraded to around 80°.

2.5. Conclusions

An atmospheric-pressure DBD plasma of gaseous with water-ethanol vapor mixture successfully enhanced the surface wettability of PTFE. Utilizing Ar and N_2 as carriers gas led to different surface finishes of PTFE. In the case of Ar, it was found that a low ethanol concentration (3%–9%) was the optimum condition for the effective hydrophilization of PTFE. The WCA dropped significantly from 115° for the original PTFE to around 20° after 10 s of plasma treatment; however, it degraded to approximately 50° after immersion in DI water. On the other hand, in the case of N_2, a similar reduction of WCA was found at ethanol concentrations of 5%, 9%, 50%, and 100%. WCA decreased from 115° to around 12° as treatment time increased up to 15 s, then it raised again to 70° as PTFE further being exposed to the plasma for 20 s. Moreover, the degradation of modified-PTFE also occurred in N_2 with water-ethanol, the WCA increased to approximately 80° after immersion in DI water. For both

working gases, the degradation of wettability indicates the limitation of PTFE surface modification.

Chapter 3. Surface Analysis of Dielectric Barrier Discharge Plasma-treated PTFE

3.1. Introduction

Super-hydrophilic surface finish of polymer materials has been reported using different kinds of technique including mechanical treatments (e.g., sandblasting, brushing), chemical treatment, and irradiation with beam of charged particles or photons [52], [53]. These treatment results in modification of surface morphology and chemical composition or both. By increasing the roughness of the surface in sub-micrometer scale and introducing polar functional groups on the surface, super-hydrophilic surface polymer can be achieved [54], [55].

Hydrophilic PTFE surface can be achieved by eliminating fluorine and creating functional groups on the surface [56]. In addition, the formation of hydrophilic functional groups during plasma treatment may lead to the generation of low-molecular-weight oxidized materials (LMWOMs), which are soluble in water. Recently, plasmas of water vapor and gas mixtures have been shown to be an inexpensive route to promote the hydrophilic surfaces on polymers. Water-vapor plasmas are dominated by H, OH radicals, O radicals, and metastable O_2, which are responsible for polymer surface functionalization [42], [57]–[61]. Sarani et al. reported efficient methods to increase polymer surface wettability by adding the correct concentration of water vapor to an Ar plasma jet. The addition of water vapor to the plasma resulted in the production of more oxygen radicals and the formation of hydroxyl groups on the polymer surface [57]. For fluorinated polymers, oxygen-rich plasmas are not sufficient to obtain a hydrophilic surface [58]. Hydrogen-rich plasmas are more favorable than oxygen-containing plasmas for improving the wettability of PTFE owing to the strong C–F chemical bonding [62].

In the previous chapter, it has been described that the wettability of PTFE improved by plasma treatment. To understand the mechanism of improvement of PTFE wettability, further analysis of the PTFE surface is necessary. The possible technique to evaluate the morphology

and chemical composition of PTFE is using an atomic force microscope (AFM) and an X-ray photoelectron spectroscopy (XPS). AFM is designated for measuring the local surface properties, e. g., roughness, height, and magnetism which belong to the group of scanning probe microscopes. The measurement is based on the interaction between the tip from the AFM with the surface of the sample results. XPS is described as one of the most useful tools to characterize plasma-treated polymers for identifying the chemical groups formed on its surface through compositional analysis and peak fitting (mostly C1s) [63]. The identification is based on the interaction of produced electrons from X-ray with the chemical structure on the polymer surface.

3.2. Objectives

In this chapter, an examination of the PTFE surface by using an AFM and an XPS will be presented. This experiment aims to obtain information on the morphology and the chemical composition of the PTFE surface treated with plasma as in the previous chapter. Morphology and chemical composition analysis is necessary for understanding the mechanism of DBD plasma treatment for PTFE, then a possible model of modification can be drawn from it.

3.3. Experimental and Methods

The morphology of PTFE surface was analyzed by AFM SPI3800N/SPA400, SII Nanotechnology Inc. (Figure 3. 1), using a tip with a diameter of 10 nm, in a dynamic force mode. The measurement was carried out using vibration frequency of ~125 kHz, vibration voltage around 1 V, I gain of 0.4 and P gain of 0.2.
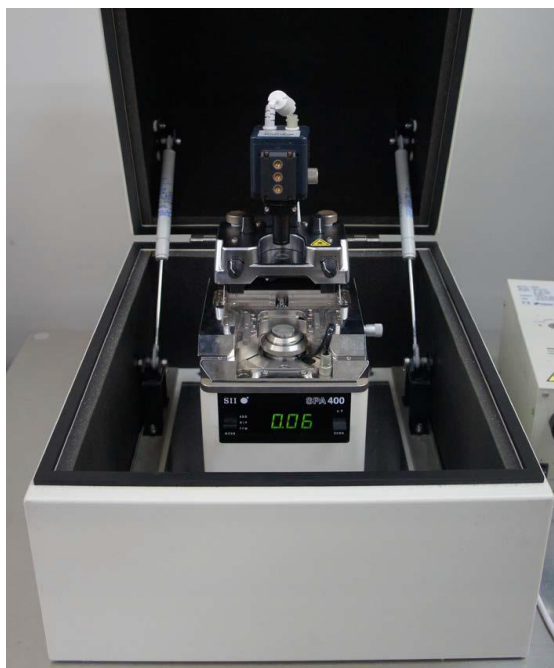
Figure 3. 1 Atomic force microscope SPI3800N/SPA40, SII Nanotechnology Inc.
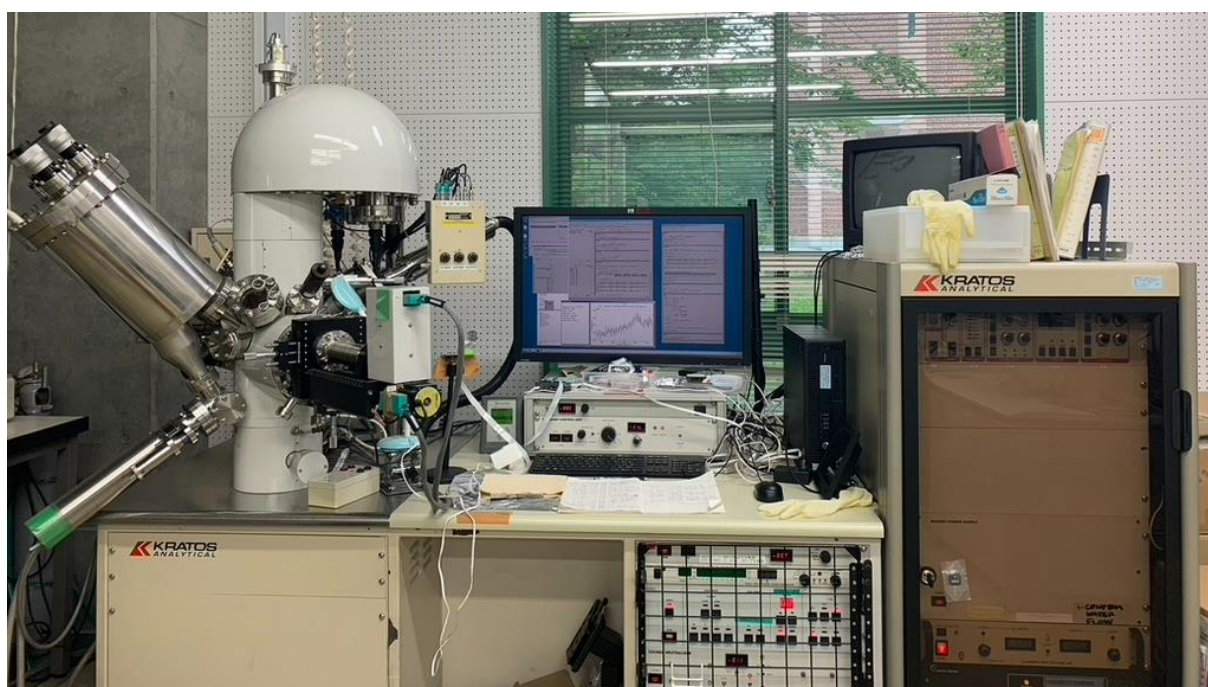
Figure 3. 2 X-ray photoelectron spectroscopy (AXIS-HS, Shimadzu/Kratos, Analytic Ltd.)

The chemical composition of the PTFE surface was measured by XPS AXIS-HS, Shimadzu/Kratos Analytical Ltd. (Figure 3 .2) using a monochromatic Al Kα X-ray radiation source (1486.6 eV). The C1s and O1s spectra were recorded with energy steps of 0.02 eV and a pass energy of 40 eV. The XPS spectra were processed using XPSPEAK41. Peak deconvolution of the C1s and O1s spectra was conducted by Gaussian-Lorentzian (70:30)

fitting after removal of the Shirley-type background, with the full width at half-maximum (FWHM) of each peak maintained at 1.5 eV. The CF_2 peak at 292.0 eV was used as a reference to determine the binding energies.

3.4. Results and Discussion

3.4.1. Morphology Analysis

Figure 3. 3 shows the surface morphology of PTFE before and after plasma treatment of Ar with water-5% ethanol. The untreated PTFE has a quite rough surface as shown in Figure 3. 3 (a). However, after plasma treatment, no significant changes were observed in the PTFE morphology (Figure 3. 3 (b-d), even after 10 s plasma treatment. It indicates that plasma treatment did not influence surface morphology modification. Based on the gas analysis in
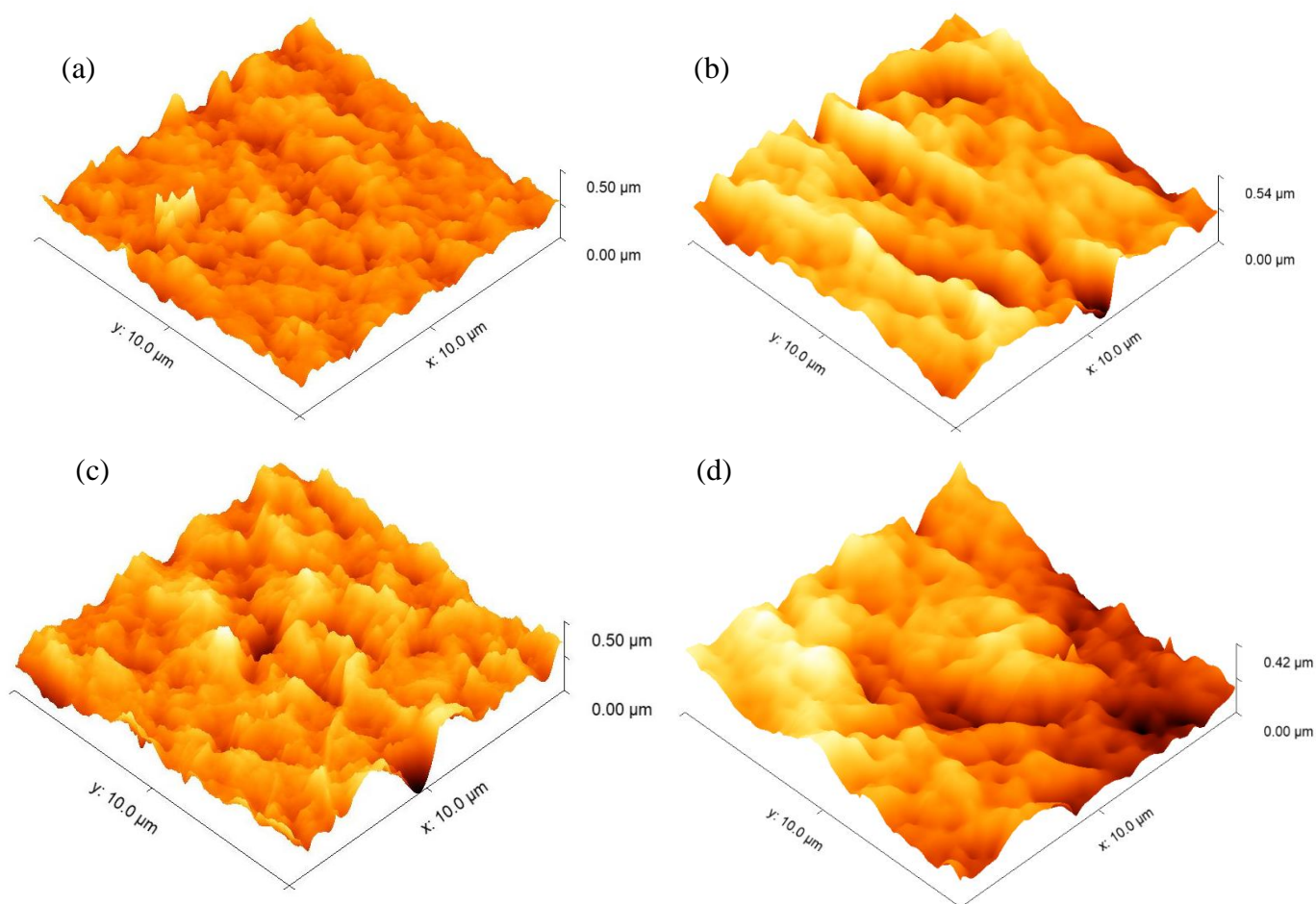
Figure 3. 3 AFM analysis for surface of (a) untreated PTFE, (b–d) plasma-treated PTFE with Ar with water–5% ethanol for treatment duration (b) 3 s (c) 7 s (d) 10 s

Chapter 2, plasma is rich in hydrogen. This plasma was not sufficient to make alteration in the PTFE morphology, especially, in rather a short time treatment duration, for instance 20 s. Hence, it suggested that improvement of PTFE wettability was not significantly affected by surface morphology.

3.4.2. Chemical Analysis

The chemical composition of PTFE before and after plasma treatment was evaluated using an XPS as shown in Figure 3. 4. The result showed that spectra untreated PTFE consists of two peaks assigned as F1s and C1s. In contrast, a peak of O1s was detected after plasma treatment of Ar with water/ethanol. Furthermore, when PTFE was treated using plasma of N_2 with water/ethanol, not only peaks of O1s but also the peak of N1s were observed on the PTFE surface. In the following sub-section, the XPS spectrum of each carrier gas will be explained in detail.
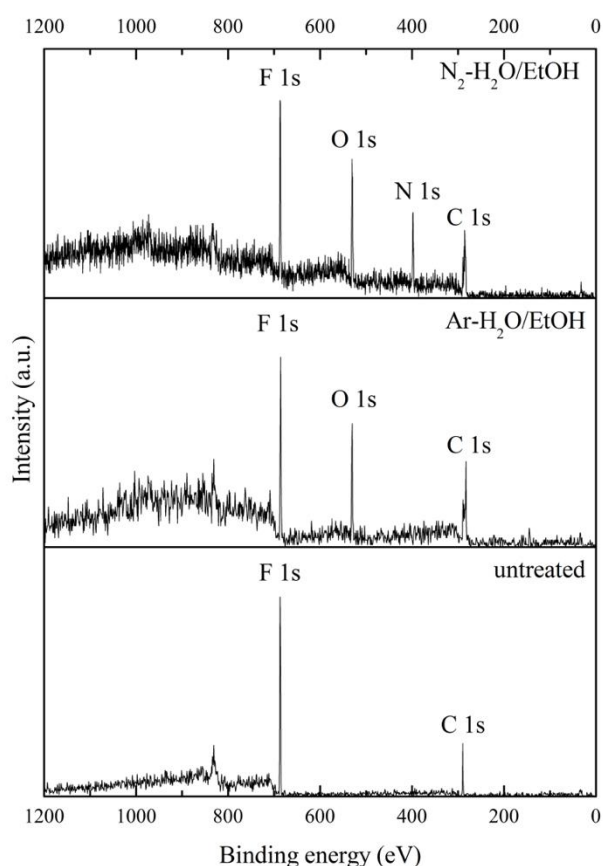
Figure 3. 4 Chemical analysis by XPS on the PTFE surface, before and after plasma treatment

3.4.2.1 Ar with water-ethanol

Figure 3. 5 displays the XPS C1s spectra of the untreated PTFE and plasma-treated PTFE for 5 s with 0%, 5%, and 100% ethanol. The C1s spectra of the untreated PTFE (Figure 3. 5 (a)), has an intense peak at 292.0 eV and a small peak at 284.0 eV, corresponding to CF_2 and π- π^* excitations, respectively. After plasma treatment, oxygen-containing functional groups, namely hydroxyl, carbonyl and carboxyl were present for all ethanol concentrations as depicted in Figure 3. 5 (b)–(d).

After plasma treatment with 0% ethanol (pure water vapor) in Ar, six additional peaks were detected, as shown in Figure 3. 5 (b): C–C/C–H at 285.5 eV, C–OH at 286.6 eV, C=O at 287.7 eV, O–C=O at 289.3 eV, C–F at 290.3 eV, and CF_3 at 292.8 eV [64], [65]. In comparison with untreated PTFE, the intensity of the CF_2 peak decreased to by approximately 50%, a significant CF_3 peak appeared, and low-intensity peaks corresponding to oxygen-containing functional groups appeared. This indicates that the approximately half of the CF_2 chain was broken, resulting in mostly fluorinated termination.

Figure 3. 5 (c) and (d) show the spectra after exposure to plasma with 5% and 100% ethanol, respectively. With the addition of ethanol vapor, fluorinated termination peaks (C–F and CF_3) did not appear in the deconvolution analysis. At a low ethanol concentration of 5%, the CF_2 peak of the original PTFE surface decreased dramatically, and the oxygen-containing functional group peaks and hydrocarbon peak increased significantly to the same level as that of the reduced CF_2 peak. This indicates that after the CF_2 chain was broken by water vapor, the surface was oxygenated, and an additional hydrocarbon layer was deposited to cover the original surface.
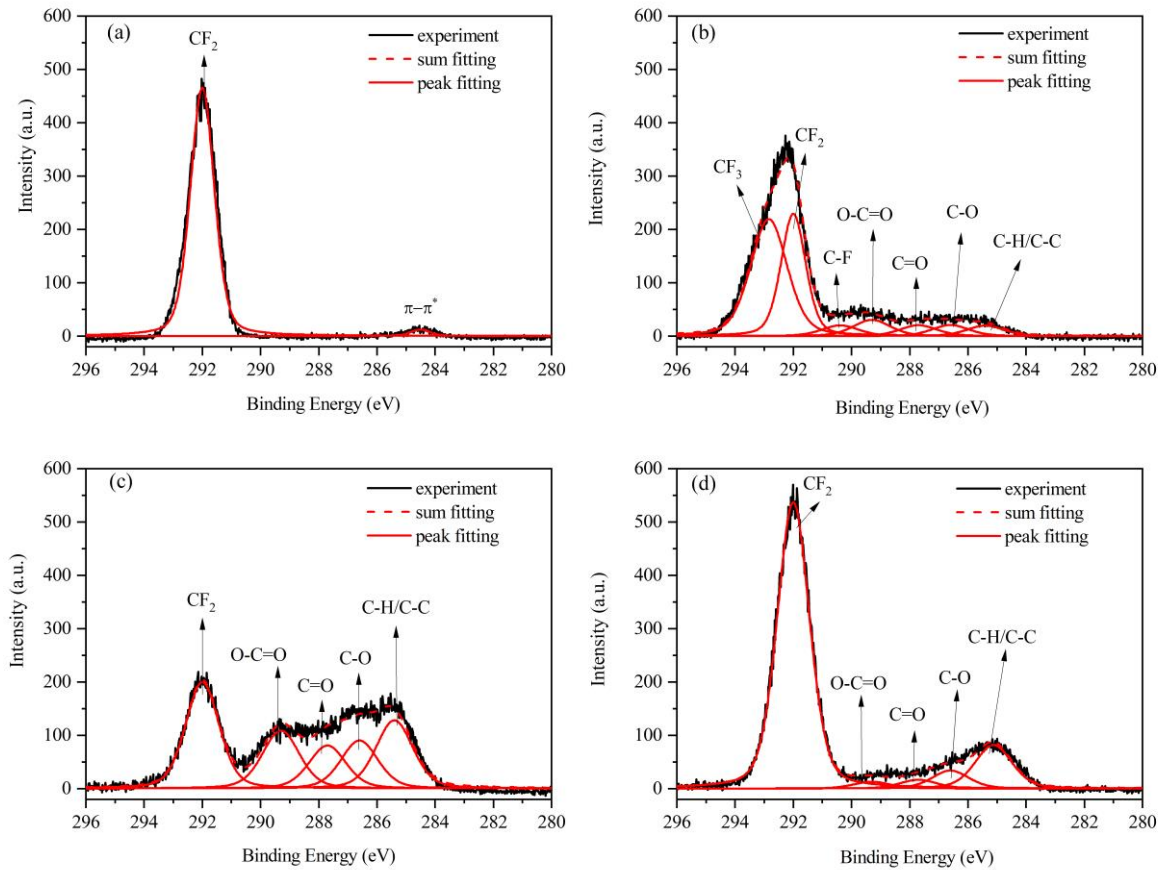
Figure 3. 5 C1s spectra of PTFE samples under different conditions: (a) untreated PTFE, (b–d) plasma-treated PTFE for 5 s with (b) Ar with water (c) Ar with water–5% ethanol, and (d) Ar with ethanol.

In the case of pure ethanol, the CF_2 peak remained at almost the same intensity as that of the original PTFE surface, while a small number of peaks corresponding to oxygen-containing functional groups appeared. This indicates that the plasma of pure ethanol in Ar could not break the CF_2 chain, which prevented the deposition of an additional layer even if enough hydrocarbon species were supplied from the decomposed ethanol in the plasma.
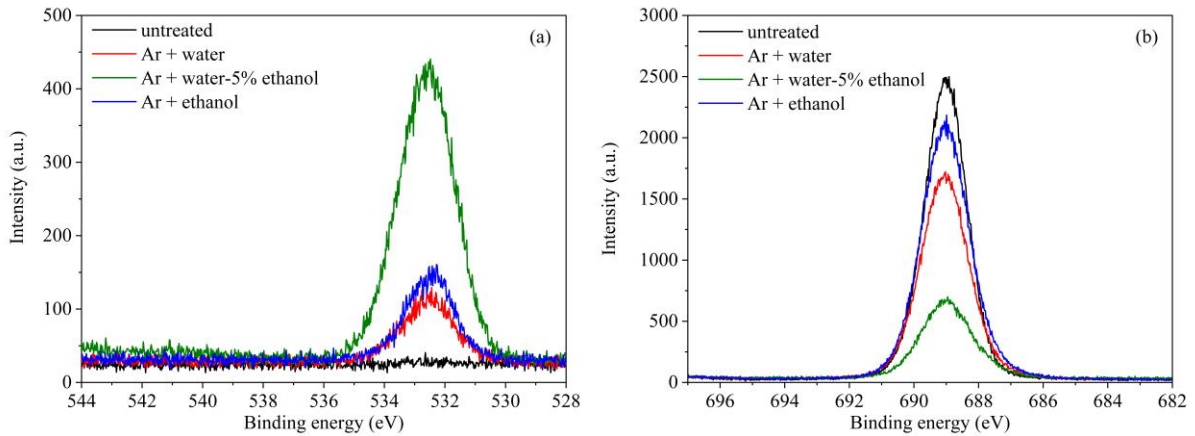
Figure 3. 6 XPS spectrum of the PTFE samples before and after plasma treatment for 5 s with different ethanol concentrations (a) O1s spectra (b) F1s spectra.

Figure3. 6 (a) shows the O1s peaks for the untreated PTFE surface and plasma-treated PTFE surfaces with different ethanol concentrations. The oxygen peak of the untreated surface was below the detection level. After the plasma treatments, a peak appeared at 532.2 eV corresponding to C–O/C=O [32]. Plasma treatment at a low ethanol concentration (5%) exhibited the highest O1s peak intensity as compared to that of pure water vapor (0%) and pure ethanol vapor (100%). The behavior of the O1s peak intensity agreed well with the analysis of the C1s peak. On the other hand, in comparison with untreated PTFE, the peak intensity of F1s spectra at 689 eV decreased after plasma treatment, as depicted in Figure 3. 6 (b). The significant reduction of F1s peak was achieved after plasma treatment of Ar with water-ethanol 5%, followed by plasma of Ar with ethanol and Ar with water, respectively.

Table 3. 1 presents the atomic ratio on the PTFE surface for five different plasma treatment conditions. The F/C atomic ratio experienced a sharp drop relative to that of the untreated PTFE after exposure to the plasma with 0% ethanol (pure water vapor). The F/C ratio decreased to 0.42 with 5% ethanol and then increased to 0.89 with 50% ethanol, where it remained almost saturated up to 100% ethanol. The O/C ratio increased dramatically up to 0.34 with 5% ethanol, whereas it was below 0.13 for other concentrations. The analysis of the C1s and O1s spectra suggests that water vapor effectively breaks the CF_2 bonds and that a small

36

amount of ethanol vapor promotes oxygenation and prevents fluorine termination. The oxygen-containing functional groups were effectively induced by a low concentration of ethanol in water, resulting in a reduced water contact angle (WCA).

Table 3. 1 Surface atomic ratio on the PTFE surface for different plasma treatment conditions.

Plasma treatment conditions	F/C	O/C
untreated	1.20	-
Ar + water	0.74	0.07
Ar + water−5% ethanol	0.42	0.34
Ar + water −50% ethanol	0.89	0.13
Ar + ethanol	0.80	0.09

XPS measurements were also performed to reveal the mechanism by which immersion in DI water degrades the WCA. Figure 8 shows the C1s and O1s spectra for the plasma-treated PTFE before and after immersion in DI water. The plasma treatment was performed using 5% ethanol for 20 s, which was a longer treatment time than that required to saturate the WCA. Comparing Figure 3. 7 (a) and Figure3. 5 (b), after the longer plasma treatment, the intensity of the CF_2 peak became smaller than the peaks of the oxygen-containing functional groups.

However, after immersion in DI water, the CF_2 peak intensity increased again, and the peak intensities of the oxygen-containing functional groups decreased, as shown in Figure 3. 7 (c). The decrease in the quantity of oxygen-containing functional groups was also supported by the reduction in the O1s peak intensity, as depicted in Figure 3. 7 (b) and (d).
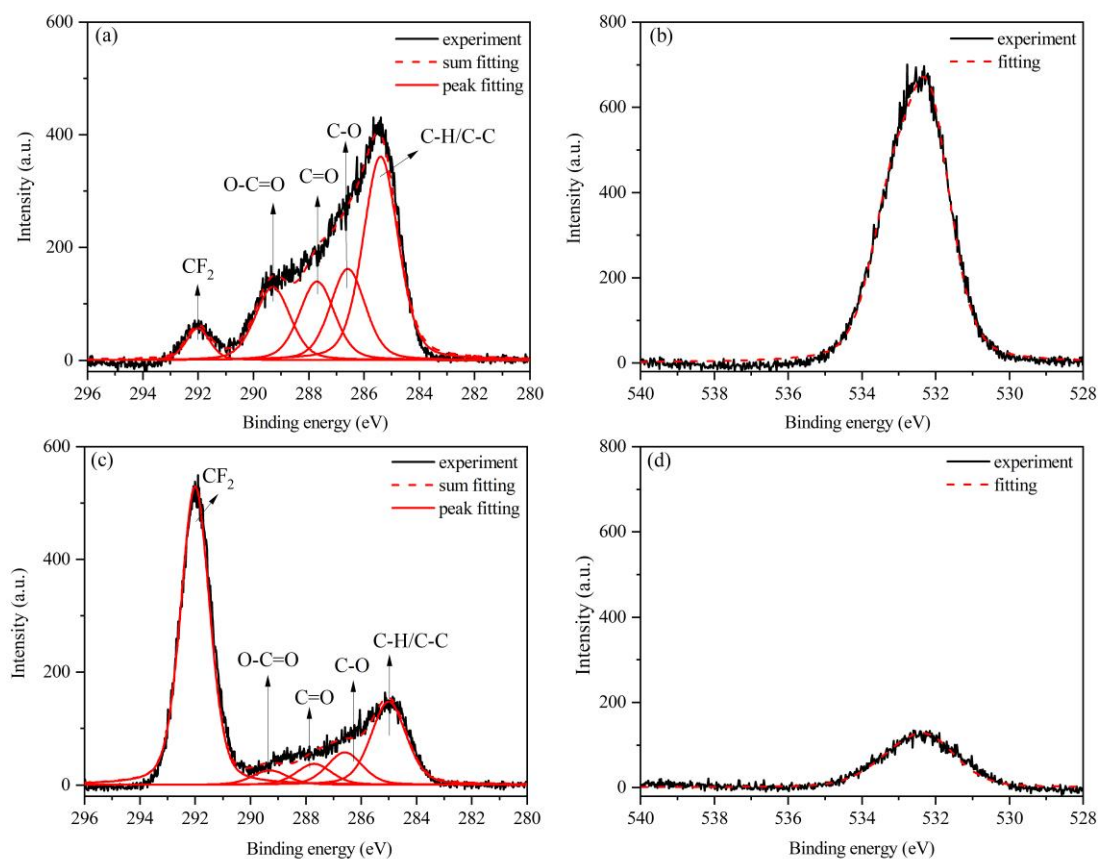
Figure 3. 7 XPS spectra of plasma-treated PTFE with Ar with water–5% ethanol for 20 s before and after immersion in DI water (a) C1s spectrum before immersion (b) O1s spectrum before immersion (c) C1s spectrum after immersion, and (d) O1s spectrum after immersion.

This implies that, during the additional treatment time, LMWOMs were deposited on the PTFE surface that was slightly modified at the beginning of plasma treatment. After plasma treatment for 20 s, the CF_2 peak intensity decreased not owing to the bond-breaking reaction but rather because the surface was covered with an LMWOM layer. After the plasma treatment, the LMWOM layer remained on the PTFE surface with residual stress, and the layer dissolved during immersion in DI water. After plasma treatment, the improved wettability was due to the LMWOM layer deposited on the PTFE. However, immersion in DI water removed the LMWOM layer and revealed a slightly modified PTFE surface, resulting in degradation of the wettability.

The chemical composition of the plasma-treated PTFE before and after immersion in DI water is summarized in Table 3. 2 as a function of treatment time. For plasma-treated PTFE

before immersion, the F/C ratio decreased with increasing treatment time (almost inversely proportional), whereas the O/C ratio experienced a sharp rise and then saturated at approximately 0.4 for more than 10 s of plasma treatment. After immersion in DI water, the chemical composition was almost remained the same for plasma treatment time of 1 s. On the other hand, for treatment times of 5 to 20 s, the F/C increased to approximately 0.9 and O/C decreased to approximately 0.05. The XPS results agree well with the WCA measurements.

Table 3. 2 Surface atomic ratio on the PTFE surface after plasma treatment of Ar with water–5% ethanol as a function of treatment time before and after immersion in DI water for 3 minutes.

Treatment time (s)	Before immersion		After immersion	
	F/C	O/C	F/C	O/C
1	1.280	0.074	1.314	0.076
5	0.420	0.343	0.909	0.052
10	0.162	0.395	0.853	0.049
15	0.074	0.392	0.841	0.048
20	0.047	0.400	0.938	0.054

It is suggested that the original PTFE surface was slightly modified during the initial 5 s of plasma treatment, resulting in stable wettability with a WCA of approximately 50°, while the deposition of the LMWOM layer began simultaneously. After more than 10 s of plasma treatment, the surface of the deposited LMWON layer exhibited excellent wettability (WCA of 20°). Based on the XPS results, an LMWON layer formed even by 5 s plasma treatment, which disappeared after immersion in DI water. While the chemical composition of the PTFE surface plasma-treated for 5 s was changed by immersion in DI water (as confirmed by the XPS analysis in Table II), the WCA values with and without the LMWON layer were approximately the same.
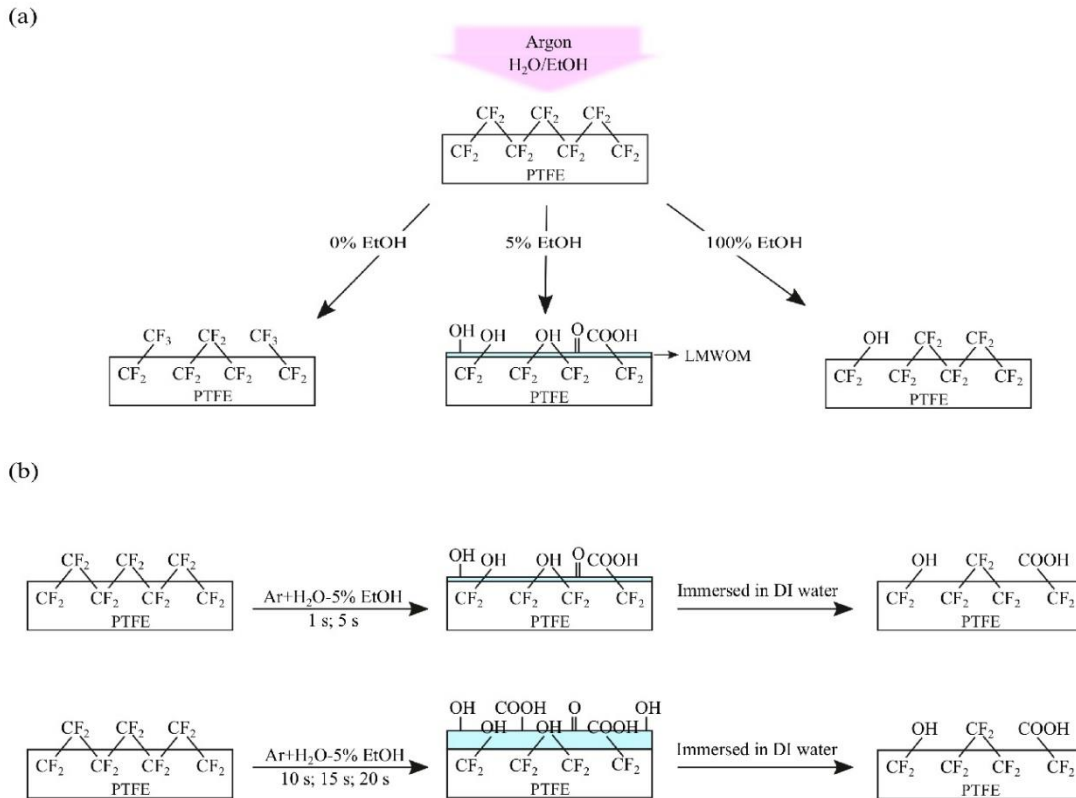
Figure 3. 8 Possible models of the PTFE modification process using an Ar with water-ethanol vapor plasma with (a) different ethanol concentration and (b) with increasing treatment time at a low ethanol concentration and immersion in DI water.

The mechanism of plasma-induced PTFE surface modification based on the results described above is depicted in Figure 3. 8. The dependence of the plasma-treated PTFE surface on ethanol concentration is shown in Figure 3. 8 (a). The original PTFE surface exhibited a continuous CF_2 chain. When the plasma treatment was performed using pure water vapor (0% ethanol) in Ar, the CF_2 chain of PTFE was broken, and most of the broken chains were terminated by fluorine as CF_3. The water vapor in the plasma was able to break the CF_2 chain but was not able to induce the formation of oxygen-containing functional groups. In contrast, for pure ethanol vapor (100% ethanol) in Ar, the plasma was dominated by hydrocarbons produced from ethanol, which resulted in less CF_2 chain breaking. The original PTFE surface without CF_2 chain breaking prevented any chemical reaction on the surface, including surface modification and thin film deposition. By combining water vapor to induce CF_2 chain breaking

and ethanol vapor to create oxygen-containing functional groups, the PTFE surface was successfully modified to achieve better wettability. To balance these surface reactions, a low ethanol concentration (3%–9 %) was suitable.

However, even at low concentrations, the deposition of the LMWOM layer proceeded continuously with increasing treatment time after the modification of the original PTFE surface, as shown in the Figure 3. 8 (b). When the treatment time was 1–5 s, the effect of the deposited LMWOM layer on the WCA was not significant compared to the modified PTFE surface itself. When the treatment time was more than 10 s, the WCA was governed by the LMWOM layer, which completely covered the surface. The LMWOM layer was easily removed by immersion in DI water, and a slightly modified PTFE surface appeared.

Plasma treatment with a low ethanol concentration induced the modification of PTFE surface and deposition of the LMWOM layer. It slightly but stably modified the PTFE surface only at the beginning of treatment but continuously deposited the LMWOM layer throughout treatment. The deposited layer prevented further modification of the surface, resulting in a limited modification of the WCA after the removal of the deposited layer in water.

3.4.2.2 N_2 with water-ethanol

After plasma treatment of N_2 with water (0% ethanol), almost there were no significant changes in C1s spectra compared to as-received PTFE shown in the blue dash line in Figure 3. 9 (a). On the other hand, by using ethanol (5% and 100%), six additional peaks were detected which assign as oxygen-containing functional groups and nitrogen-containing functional groups as shown in Figure 3. 9 (b-c) [63]. Among these two conditions, the most functional groups were found in 5% ethanol concentration. Furthermore, the CF_2 peak at 292.0 eV experienced a reduction after plasma treatment. It reduced up to around 1/4 and 1/2 of the original PTFE for 5% ethanol and 100% ethanol, respectively.
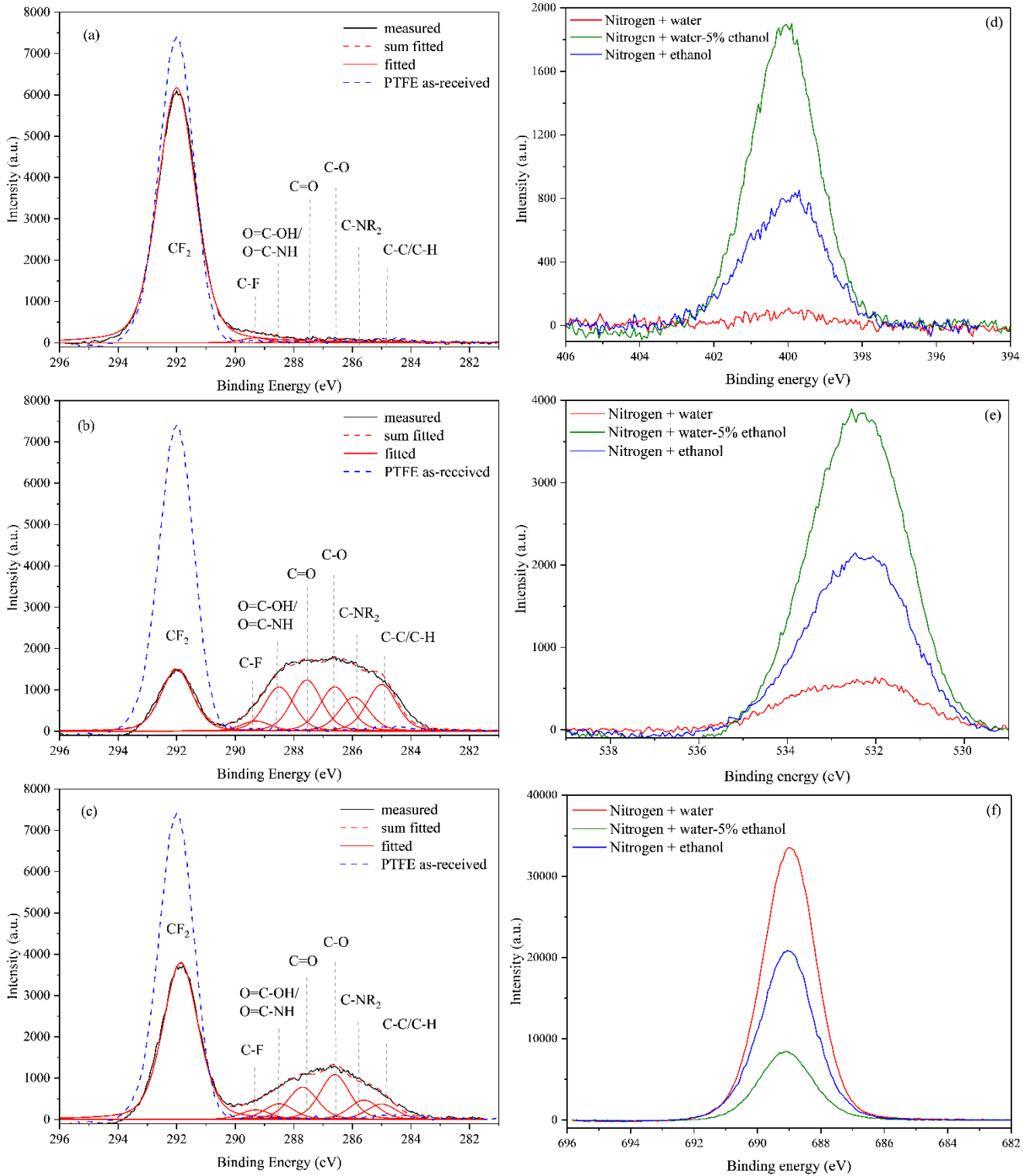
Figure 3. 9 XPS spectrum of the plasma-treated PTFE under different conditions: (a-c) C1s spectrum (a) N_2 with water (b) N_2 with water-5% ethanol (c) N_2 with ethanol (d) N1s spectrum (d) O1s spectrum (f) F1s spectrum

The result of the C1s spectrum was supported by N1s, O1s, and F1s spectrum as shown

in Figure 3. 9 (b-d). The highest peak intensity of N1s and O1s was found at N_2 with water-5%

ethanol, followed by 100% ethanol and 0% ethanol, and vice versa for F1s spectra. It indicates

42

that the addition of ethanol vapor as a working gas induced the formation of functional groups, whereas water vapor only plasma was not sufficient to facilitate any chemical reaction.

Table 3. 3 Surface atomic ratio on the PTFE surface for different plasma treatment conditions.

Plasma treatment conditions	F/C	O/C	N/C
untreated	1.70	-	-
N_2 + water	1.69	0.08	0.01
N_2 + water −5% ethanol	0.47	0.41	0.26
N_2 + water −50% ethanol	0.69	0.27	0.22
N_2 + ethanol	1.07	0.22	0.12

The alteration of atomic ratio on the PTFE surface for five different plasma treatment conditions is presented in Table 3. 3. The F/C atomic ratio remained the same value relative to that of the untreated PTFE with the addition of a small amount of oxygen and nitrogen after exposure to the plasma with 0% ethanol (pure water vapor). As ethanol concentration increased, the F/C ratio decreased sharply to 0.47 with 5% ethanol and then increased to 0.69 and 1.07 with 50% ethanol and 100% ethanol, respectively. Furthermore, the O/C ratio increased dramatically up to 0.41 with 5% ethanol, whereas it was around 0.25 for other concentrations. For the N/C ratio, 5% ethanol and 50% ethanol showed almost similar values at 0.25 whereas it reduced for 100% ethanol at 0.12. This result was not well agreed with the WCA of plasma-treated PTFE. This suggests that improvement of wettability was caused by the formation of functional groups, yet it was not proportionally correlated to the atomic ratio.

Figure 3. 10 shows C1s spectra of plasma-treated PTFE of N_2 with water–5% ethanol as a function of treatment time. It was clearly observed that, as treatment time increased, the CF_2 bonding peak at 292.0 eV decreased until disappeared after being treated for 15 s. Then, it appeared again when plasma treatment was performed for 20 s. In contrast, the peak area of

functional groups increased by increasing plasma duration. The details area ratio of each functional group in C1s spectra is listed in Table 3. 4. Increasing time for plasma treatment, resulted in decreasing of the CF_2 bond area ratio from 65 to around 2 after 15 s treatment then it increased again to 11.79 when treated for after 20 s. On the other hand, the C-F bond kept increasing with increasing treatment time up to 20.34 after 20 s plasma exposure. Furthermore, the created functional groups have the same tendency which increased over time and then dropped in longer treatment time. A significant reduction of the CF_2 peak suggests that the creation of polar groups on the PTFE surface occurs through thin film deposition rather than modification. Moreover, by increasing treatment time, the PTFE surface temperature increased because of high plasma power density. This might lead to deformation and re-orientation of the polar groups to the bulk material, which can be observed by re-appearing of CF_2 bond peak and decreasing of functional groups after exposing plasma for 20 s.
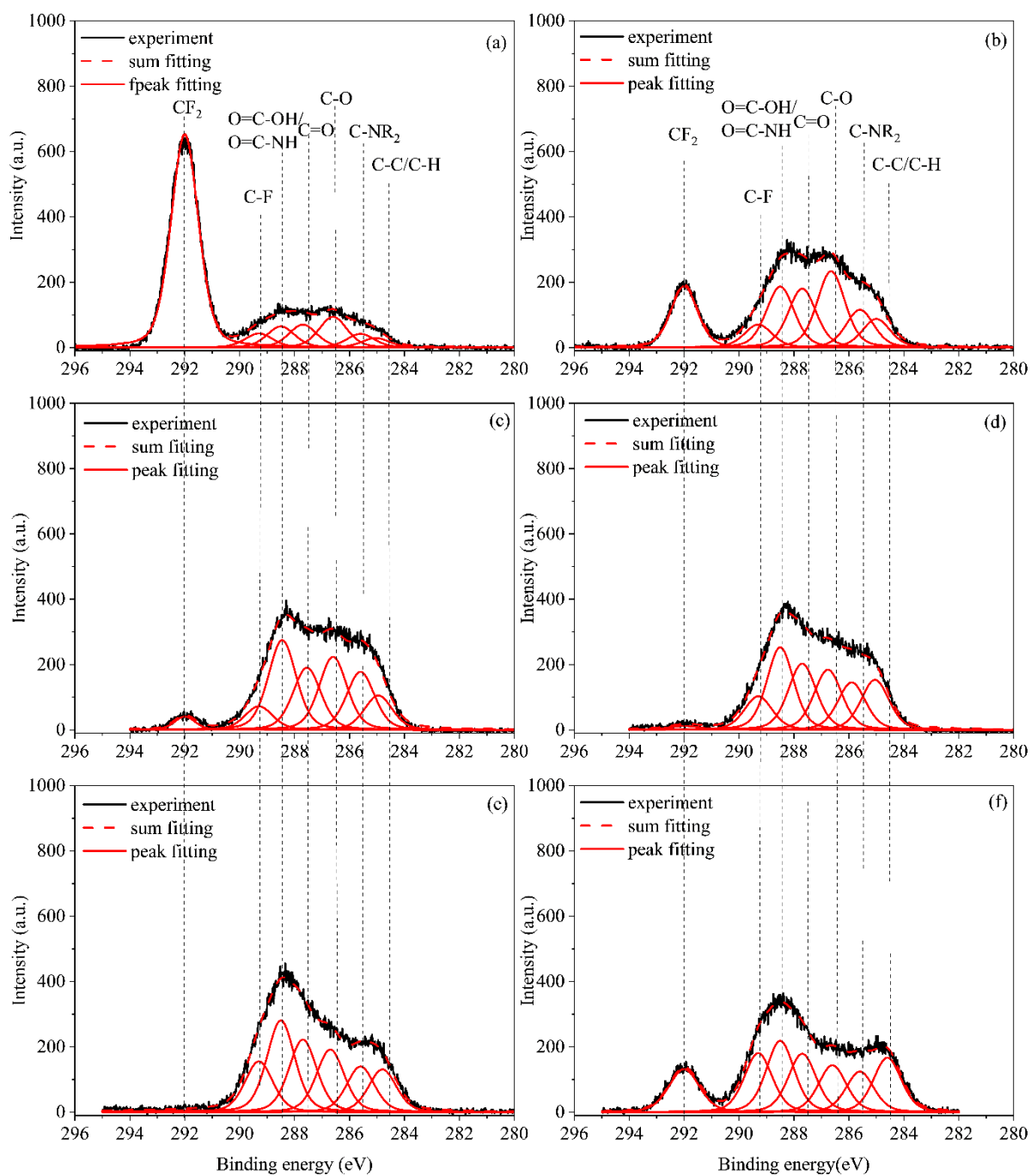
Figure 3. 10 C1s spectrum of plasm-treated PTFE of N$_2$ with water–5% ethanol for treatment time of (a) 1 s (b) 5 s (c) 7 s (d) 10 s (e) 15 s (f) 20 s.

Table 3. 4 Area ratio of C1s component on the PTFE surface after plasma treatment of N_2 with water–5% ethanol as a function of treatment time

Treatment time	$C-F_2$	C-F	O-C=O/ O-C=N	C=O	C-O	C-N
1	65.102	4.387	6.569	7.151	9.588	4.250
5	16.967	6.677	17.716	17.142	22.206	10.981
7	2.826	6.737	25.559	17.716	20.815	16.528
10	1.322	9.850	23.182	19.428	17.634	13.906
15	2.312	13.565	24.442	19.364	16.718	12.185
20	11.786	20.338	17.803	14.589	11.733	10.137
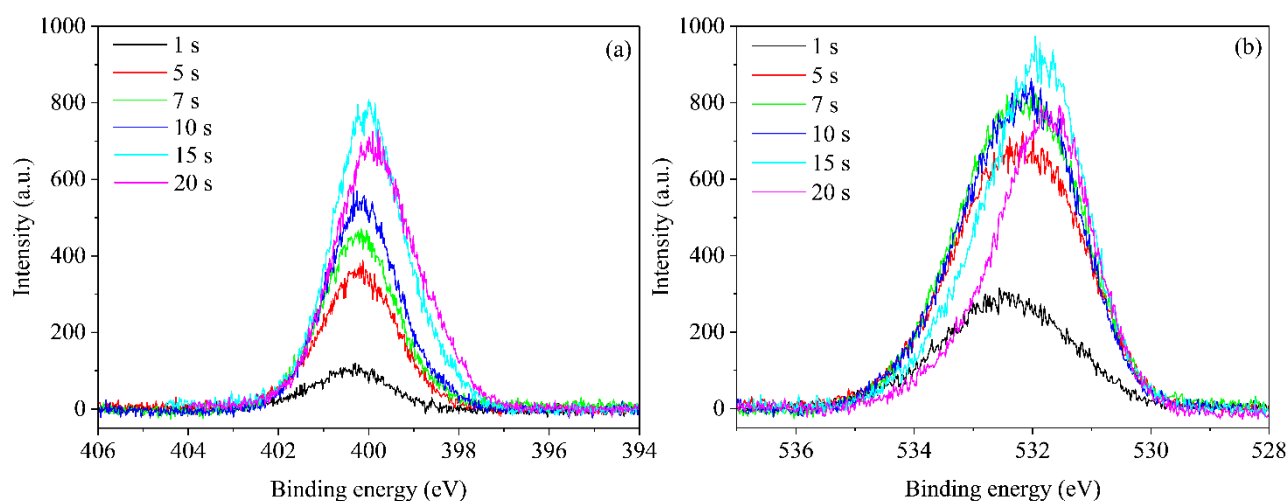
Figure 3. 11 XPS spectrum of plasm-treated PTFE of N_2 with water–5% ethanol as a function of treatment time (a) N1s spectrum (b) O1s spectrum

Figure 3. 11 depicts N1s and O1s spectra of plasma-treated PTFE as a function of treatment duration which changes in a similar manner. As treatment time increased, the intensity of the peak increased, yet it decreased slightly at 20 s treatment duration. In addition, for the N1s peak, the full-width-half-maximum (FWHM) became wider indicating a contribution of amine and amide groups bonding. For O1s, different FWHM suggested the different contributions of C-O and C=O bonding.
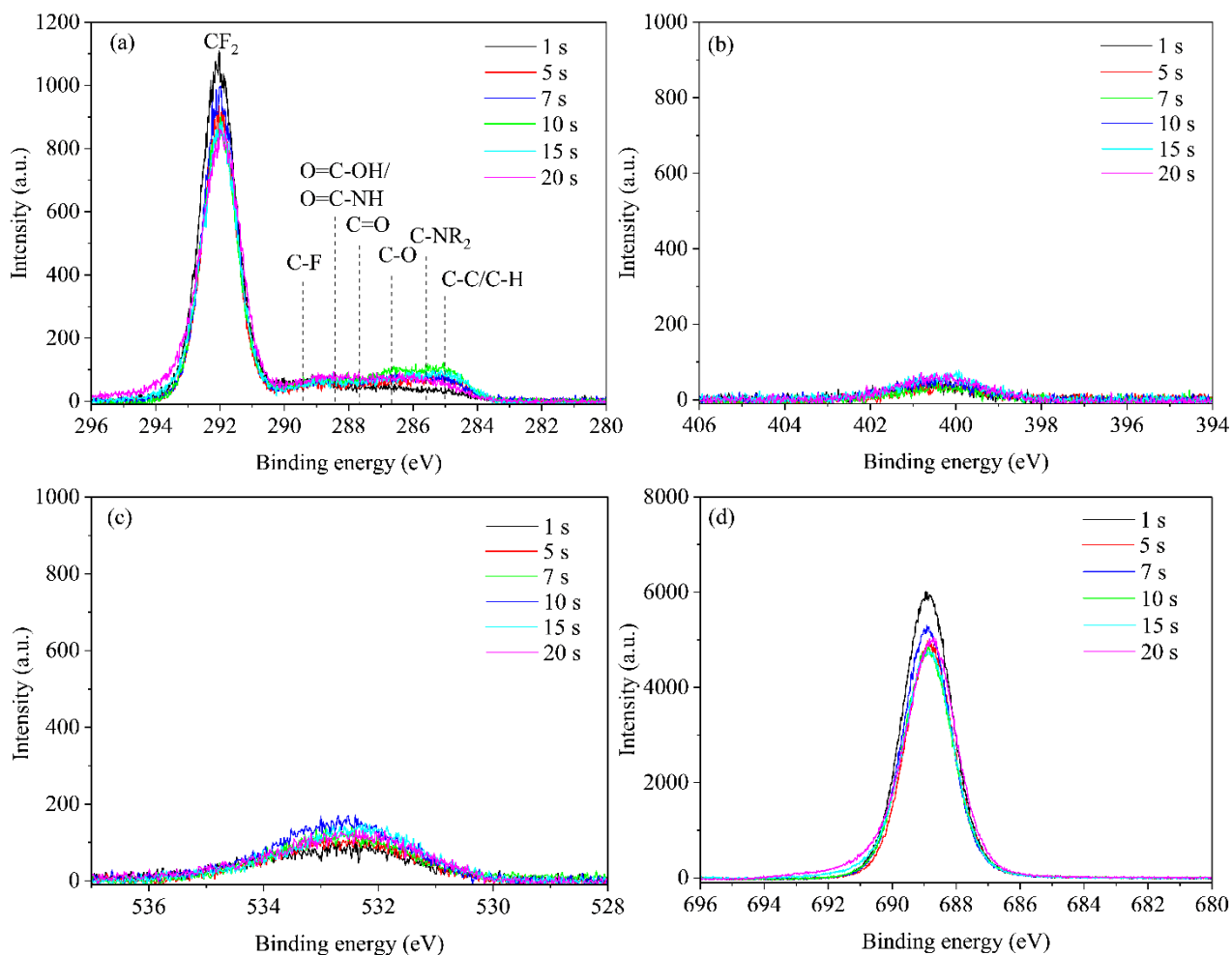
Figure 3. 12 XPS spectrum of plasma-treated PTFE with N_2 with water-5% ethanol after immersion in DI water for different treatment time (a) C1s spectrum (b) N1s spectrum (a) O1s spectrum (b) F1s spectrum.

The XPS spectrum for plasma-treated PTFE after immersing in DI water is shown in Figure 3. 12. After immersion in the DI water, the C1s, O1s, N1s, and F1s spectrum had an almost similar area of the peak regardless of the plasma treatment duration. It indicates that polar groups formed on the PTFE surface after plasma were not stable owing to the deposition of a thin layer. The detailed alteration of the atomic ratio of the plasma-treated PTFE before and after DI-water immersion is presented in Figure 3. 13. Referred to the as-received PTFE, after 1 s plasma treatment, no significant difference in the F/C atomic ratio was observed. However, a dramatic dropped in F/C ratio was observed after 3 s exposure of plasma to 0.348 and kept decreasing with increasing treatment time to 0.082 for 15 s treatment time. Moreover, long plasma treatment (20 sec) resulted in the F/C ratio increasing again. On the other hand, by

47

increasing treatment time, the amount of oxygen and nitrogen increased also, as shown by increasing O/C and N/C ratios up to 0.513 and 0.642, respectively at 15 s treatment. Furthermore, in the case of 20 s treatment time, the atomic ratio was slightly dropped to 0.375 for the O/C ratio and 0.575 for the N/C. However, after being immersed in DI water, regardless of the plasma treatment time, PTFE has the same atomic ratio of F/C, O/C, and N/C resulting in degradation of WCA. It indicates that the wettability of modified-PTFE was affected by the chemical composition.
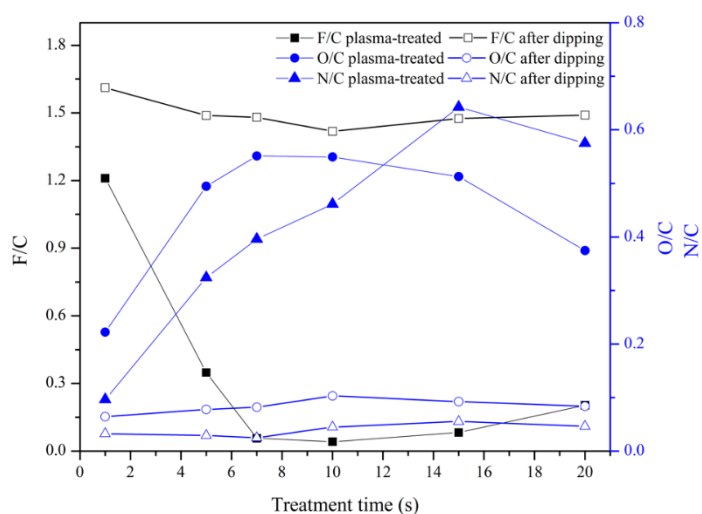
Figure 3. 13 Surface atomic ratio on the PTFE surface after plasma treatment of N_2 with water–5% ethanol as a function of treatment time before and after immersion in DI water for 3 minutes.

The mechanism of plasma-induced PTFE surface modification based on the results described above is depicted in Figure 3. 14. The dependence of the plasma-treated PTFE surface on ethanol concentration is shown in Figure 3. 14 (a). The original PTFE surface exhibited a continuous CF_2 chain. When the plasma treatment was performed using pure water vapor (0% ethanol) in N_2, plasma was not sufficient to cleave the CF_2 chain. The original PTFE surface without CF_2 chain breaking prevented any chemical reaction on the surface, including surface modification and thin film deposition. In contrast, adding ethanol facilitated CF_2 chain breaking and then induced the formation of polar groups as well as the deposition of a thin layer/LMWOM on the PTFE surface. In the case of pure ethanol vapor (100% ethanol) in N_2,

the plasma was dominated by hydrocarbons produced from ethanol, which resulted in less CF_2

chain breaking and less creation of functional groups.

(a)

(b)
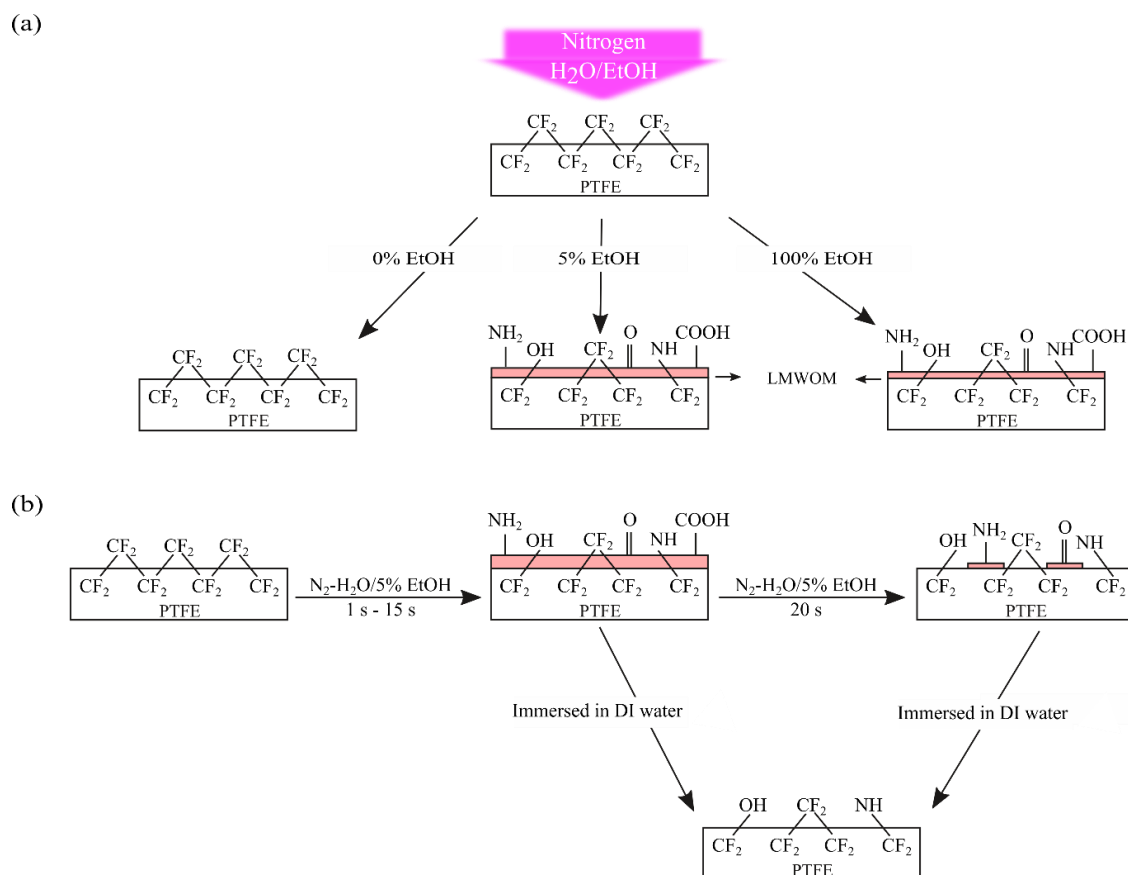
Figure 3. 14 Possible models of the PTFE modification process using a N_2 with water-ethanol vapor plasma (a) in different ethanol concentration and (b) with increasing treatment time at a low ethanol concentration and immersion in DI water.

During plasma treatment using 5% ethanol, surface modification and thin film

deposition occurred at the same time. However, thin film deposition was more dominant and

gradually covered the original PTFE surface which prevented the surface modification. The

deposition of the LMWOM layer proceeded continuously with increasing treatment time which

completely covered the PTFE surface after 15 s, as shown in Figure 3. 14 (b). When the

treatment time was further increased to 20 s, reorientation or deformation of this thin layer

happened due to rising in surface temperature. The WCA was governed by the LMWOM layer,

which completely covered the surface. Furthermore, this LMWOM layer was easily removed

by immersion in DI water, and a slightly modified PTFE surface appeared.

3.5. Conclusions

After plasma treatment, the surface morphology of PTFE was not significantly changed. In contrast, the chemical composition was greatly altered after plasma treatment which corresponds to the improvement of PTFE wettability. The oxygen-containing functional groups and nitrogen-containing functional groups were formed on the PTFE surface. The functional groups formed on the PTFE surface depended on the ethanol concentration and plasma treatment duration. The possible model was proposed to describe the interaction between plasma species and the PTFE surface. In the case of Ar as a gas carrier, the pure water vapor plasma induced the breaking of the CF_2 chain, resulting in more fluorinated terminations (such as CF_3), whereas the pure ethanol vapor plasma was not effective in initiating surface reactions. The low ethanol concentration plasma modified the PTFE surface by breaking the CF_2 chain and introducing oxygen-containing polar groups (C–OH, C=O, and O=C–OH), and simultaneously deposited a LMOWM layer on the modified surface. After removal of this layer by immersion in water, a stably modified PTFE surface appeared with a WCA of around 50°. In the case of N_2 as the gas carrier, the reduction of WCA was due to the deposited LMOWM layer on the PTFE surface rather than surface modification. It was shown by the degradation of WCA to the same value at 80° after immersion in DI water regardless of the plasma treatment duration. In addition, the CF_2 peak decreased significantly till disappeared after plasma treatment which suggests that LMWOM layer fully covered the original surface of PTFE.

Chapter 4. Generation of atmospheric pressure gas discharge induced by photoemission

4.1. Introduction

Recent studies on atmospheric-pressure plasma (APP) have led to the development of low-temperature plasma, which has a wide range of applications including chemical conversion, biomedical engineering, agriculture, and disinfection [19], [29], [66]. APP is a cost-effective alternative to existing low-pressure plasma because it does not require a vacuum system.5,6 Furthermore, APP can produce multiple excited and ionized species, particularly reactive oxygen species and reactive nitrogen species (RONS). These play an important role in plasma medicine, such as in the treatment of cancer and skin diseases [67]–[69].

However, gas discharge generation at high pressures experiences issues in terms of stability and uniformity. Typically, gas breakdown occurs via filamentary discharge, streamer discharge, and microarc discharge. In addition, the difficulty for generating stable APP includes, but not limited to, a few options of discharge gases (He, Ar, N_2), high-flow-rate gas jets, current limitations due to dielectric barrier discharge, and the use of nano pulse power sources [14]. These constraints limit the applications of atmospheric-pressure plasma which is necessary to be addressed.

The breakdown voltage of gas discharge can be expressed using Paschen's law as a function of parameter pd, which is the product of pressure p and discharge gap d. At a high pressure, a small discharge gap is suitable for the easy ignition of discharge. Moreover, the volume of a discharge space decreases according to Paschen's law, and current becomes concentrated in a small cross section. In the small discharge space, the probability of accidental ionization by a cosmic ray becomes too small to supply primary electrons. Thus, to use APP in such a space, it is effective to intentionally supply free electrons via field-emission [70] and photoemission.

Photoemission-assisted low-pressure plasma generation was reported in previous studies for synthesizing nano graphite and diamonds as well as flattening material surfaces [71]–[74]. A DC gas discharge was generated using photoelectrons from a substrate irradiated with vacuum UV light (wavelength: 172 nm) from a Xe excimer lamp. The plasma was generated from the photoelectrons in the Townsend discharge mode. Glow-like plasma was formed even in the Townsend mode through the emission of high-density photoelectron current using a UV light source with sufficient photon energy for the work function and high-power density.

A back-illuminated gold thin film as a photocathode was used in electron beam lithography, electron guns, and optical fiber [75]–[78]. It was reported that a stable photoemission was obtained by back-illuminating gold thin film using a high-power 257 nm laser (200 mW) even when was operated in air or less vacuum condition [75]. However, the quantum efficiency of photoemission depended on the thickness of the gold thin films. As reported also in [76], a 266 nm UV femtosecond laser was used for the back-illuminated gold thin-film photocathode. As a result, the optimum thickness of the gold photocathode was confirmed to be 10 nm at a photocurrent of 3 nA. A. Casandruc (2016) utilized photoemission mechanism to produce free electron for optical fiber application [78]. A Gold thin film of 30 nm thickness was back illuminated with femtosecond laser of 257 nm wavelength. The result showed that photocurrent proportional with applied laser power which suggested that single-photon photoemission being the predominant electron emission

4.2. Objectives

The objective of this work is to address the limitations on the generation of stable APP which highly demand in medical and agriculture applications. A novel approach was developed for generating stable atmospheric-pressure gas discharge using a back-illuminated thin-film gold photocathode. In addition, to study the mechanism of photoemission-induced atmospheric

pressure gas discharge as well as the effect of UV photon energy, UV power density intensity and working gas on the gas discharge generation.

4.3. Experimental and Methods

A thin gold photocathode with a size of 25 mm × 26 mm and a thickness of 9 nm was deposited on quartz slide glass with dimensions of 76 mm × 26 mm × 1 mm using a conventional DC magnetron sputtering apparatus. As shown in Figure 4. 1, a U-shaped silicon rubber sheet was inserted as a spacer between the photocathode and an anode plate of Al alloy to create a discharge cell with a gap of 1 mm and a gas flow channel with a width of 15 mm. Ar or air was flown from a gas cylinder or air compressor, respectively, into the discharge cell through a mass flow controller (MFC) at a flow rate of 250 sccm.
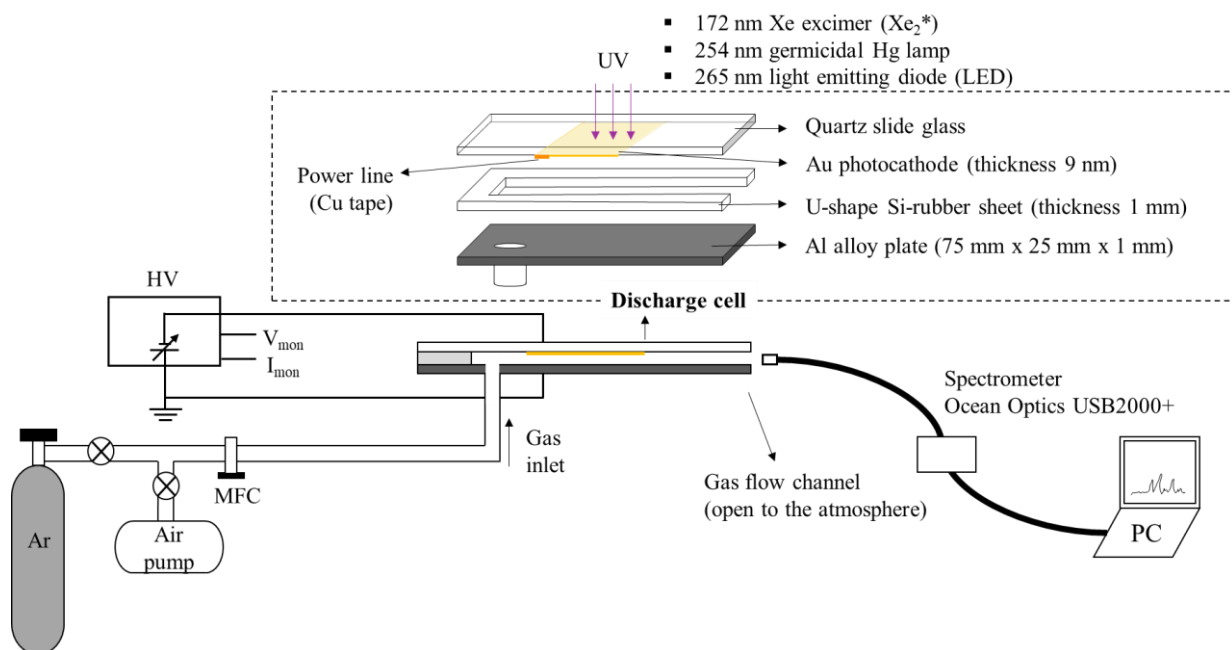
Figure 4. 1 Experimental setup of atmospheric pressure gas discharge induced by photoemission

The photocathode was externally illuminated through the quartz glass using three UV light sources: a 172 nm Xe excimer (Xe2*) lamp (ORC Manufacturing Co., Ltd., OEL-172-040FSS), a 254 nm germicidal Hg lamp (Toshiba, GL4), and a 265 nm light emitting diode (LED) (Nikkiso, Deep UV-LED). The Xe excimer and Hg lamps were operated at 37 kHz and 60 Hz, respectively, and the LED was operated using DC. The lamps were expected go pulsate,

resulting in the pulsation of the photoemission current and discharge current. However, the current was measured as the time-averaged DC.
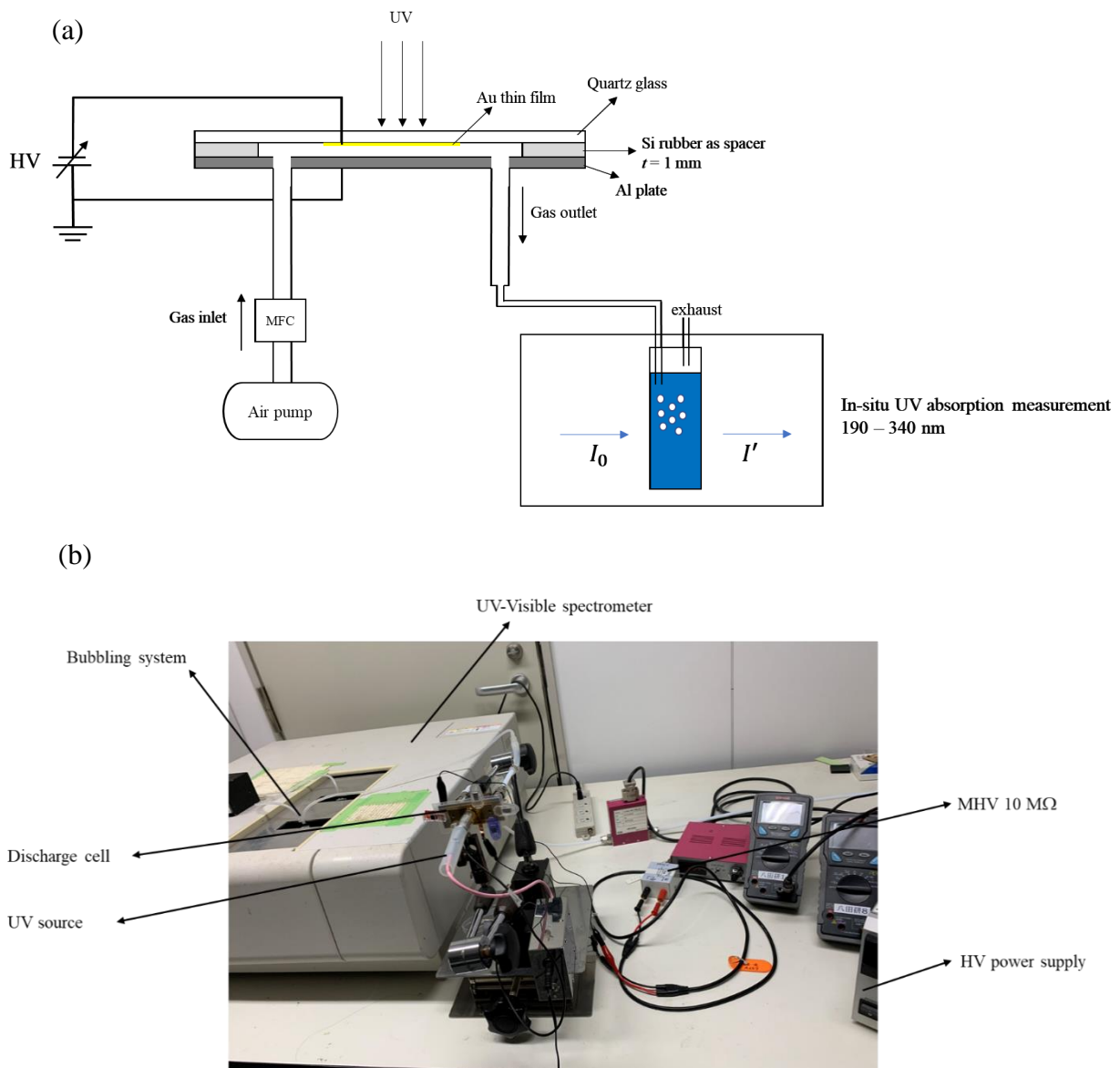
Figure 4. 2 Experimental setup of UV absorption measurement of atmospheric pressure gas discharge induced by photoemission (a) schematic (b) photo.

The illuminated power density of the Xe excimer lamp was measured at the center as the maximum of the irradiation profile using a 172 nm UV monitor (Iwasaki Electric Co., Ltd., Diamond VUV monitor EVUV-200). The irradiated power density was varied by changing the distance between photocathode and excimer lamp. When the Xe excimer lamp was in direct contact with the photocathode quartz glass (0 mm), the working area of the photocathode was limited to a diameter of 15 mm on the gold film owing to the size of the lamp. By increasing

the distance, the working area of photocathode increased until it covered the entire area of the gold film (25 mm × 15 mm).

A high DC negative voltage was applied to the photocathode, and the anode was grounded. The voltage and current were monitored using the output of the power source. The optical emission spectra of the generated plasma were observed from the open end of the discharge cell using a spectrometer (Ocean Optics, USB2000+) through an optical fiber.

Figure 4. 2 depicts a setup measurement of UV absorption spectroscopy for dissolved gas in water. A conventional double-beam UV-VIS spectrophotometer (Hitachi U-3900) with cuvettes (Hellma Analytics QS-101) were used to measure the optical absorption in deionized water (DI water) with an optical path of 10 mm. The measurement method and the data analysis referred to our previous study [71,72]. The absorption spectra were measured only in the UV region between 190 – 340 nm with a spectral resolution of 0.2 nm and scan speed of 120 nm/min.

4.4. Results and Discussion

4.4.1. Gold thin film optimization

Prior to the generation of atmospheric pressure gas discharge induced by photoemission, photocathode was prepared using gold thin film deposited onto quartz glass. A DC magnetron sputtering was utilized to fabricate gold thin film as shown in Figure 4. 3 which has deposition rate of 18 nm/min. It has been mentioned in the previous study that photocurrent under back-illumination is depended by thickness of gold thin film. Initially, photocurrent will increase as
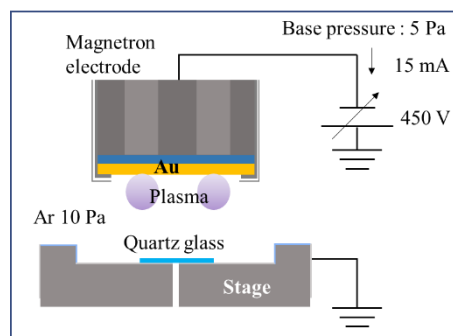
Figure 4. 3 Schematic of DC magnetron for gold thin film deposition

thickness of gold thin film increase due to rising in absorption of the light of the film. Then, as the film becomes thicker than both the optical absorption depth and the scattering mean free path, the photocurrent will decrease. In this study, several different thickness of gold thin films were prepared by varying the deposition time resulted in thickness of 3 nm to 27 nm.

Figure 4. 4 depicts the dependency of the gold thin film thickness on the UV absorbance and the UV transmittance. The result showed that there was no significant peak detected in all different thickness of gold thin film. It was suggested that gold thin films absorb UV light ranging 190 nm – 340 nm with almost similar coefficient. However, by increasing the thickness of gold thin film, the absorbance increased, and the transmittance decreased.
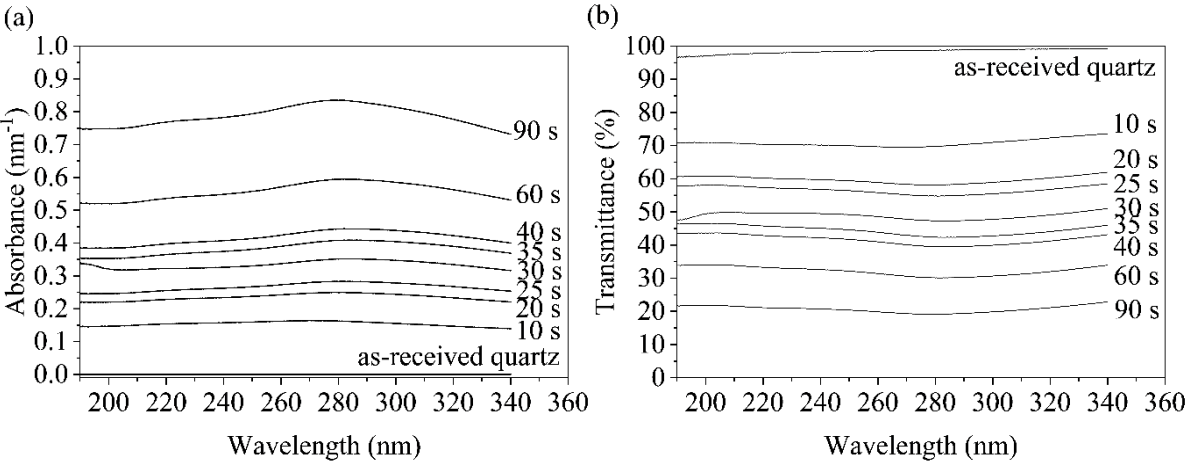
Figure 4. 4 Optical properties of gold thin film with different thickness (a) UV absorbance (b) UV transmittance
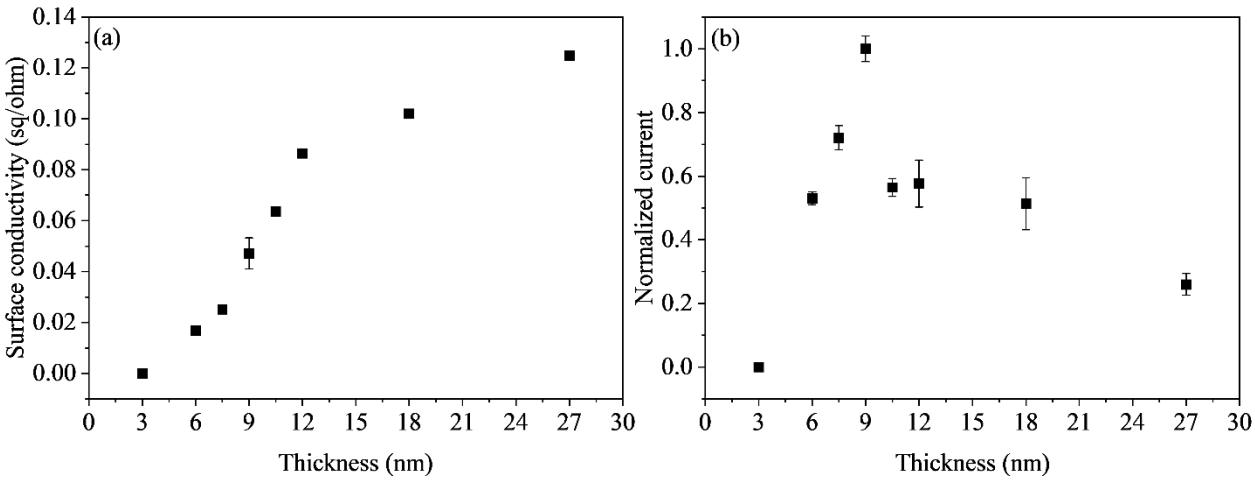
Figure 4. 5 Electrical properties of gold thin film as a function of thickness (a) surface conductivity (b) photocurrent

The electrical properties of gold thin film were analyzed by measuring the surface conductivity and the photocurrent as shown in Figure 4. 5. When thickness of gold thin film was 3 nm (10 s deposition time), it was not conductive enough owing 0 surface conductivity (Figure 4. 5 (a)). As the thickness of gold thin film increased, the surface conductivity increased then showed saturation tendency. The photocurrent was measured by back-illuminating thin film with an excimer lamp 172 nm. The result of photocurrent as function of gold film thickness is presented in Figure 4. 5 (b). By increasing thickness of gold thin film, the photocurrent increased, then gradually decreased. This pattern well agreed with the previous published results. The maximum photocurrent was achieved around 173 nm at 9 nm, indicated as the optimum thickness of photocathode.

4.4.2. Effect of the UV source

Figure 4. 6 depicts the current–voltage relationships for the gas discharge under atmospheric-pressure Ar gas with the different UV light sources and without UV illumination. When the 172 nm UV was used, the current started increasing steadily when the voltage exceeded 500 V, and a steady discharge of approximately 30 μA was obtained at 1500 V. The stable DC discharge was sustained for a long time at voltages below 1500 V. When the voltage was increased further, sparks were randomly generated around the edges of photocathode, and discontinuously large current values were observed (not shown for the 172 nm case in Fig. 4. 6), resulting in visible damage to the photocathode. Hence, the stable DC discharge conditions had an upper limit of the voltage or current. Within the limit of no-spark discharge, the gold

thin film photoelectrode was not damaged and could be operated for a long time with high reproducibility.
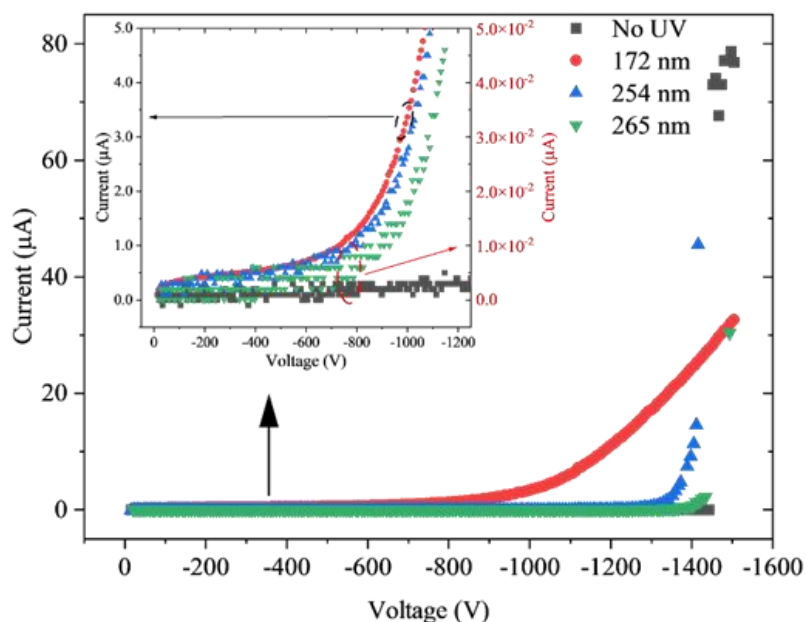
Figure 4. 6 Current–voltage characteristics of photoemission-induced atmospheric-pressure Ar discharge with different UV light sources.
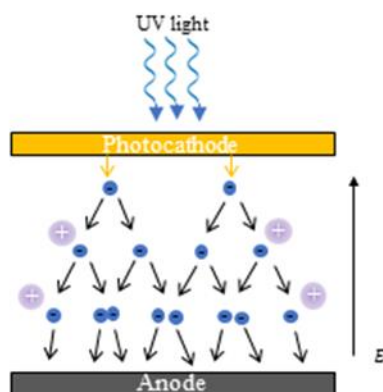
Figure 4. 7 Possible model of gas breakdown in photoemission-induced atmospheric pressure gas discharge.

The current–voltage characteristics of the stable DC discharge were possibly divided into four distinct regions. 1) First, the current increased with the voltage up to 200 V. 2) Then, the current was saturated. 3) Next, approximately 500 V onwards, the current increased exponentially with the voltage. 4) Finally, above 1000 V, the current increased proportionally with the voltage. In region 1, photoelectrons were emitted and transported in the atmospheric-pressure gas. The current increased with the voltage until the extraction voltage required for emission and electric field required for transport were sufficient. In region 2, the current slightly

increased with the voltage owing to the enhancement of electron transport, and the photoemission was almost saturated. In region 3, like the Townsend discharge, photoelectrons were accelerated in the electric field, and the current increased through avalanche ionization as shown in Figure 4. 7. In region 4, the exponential increase in current due to avalanche ionization was limited because a resistance component appeared in the discharge space. The saturated photoemission current considered in region 2 was approximately 0.5 µA, and the discharge current approached to 30 µA at 1450 V. Hence, the photoemission current amplified by approximately 60 times in the electric field.

In case of no UV illumination, the observed current was insignificant up to a voltage of 1450 V. When the voltage was increased further, a discontinuous and large current (70 µA) abruptly appeared, resulting in damage to the photocathode. The observed current value was not the actual peak current of the spark discharge, but the time-averaged value obtained through DC measurement.

When the 254 nm and 265 nm sources were used, as shown in the inset of Figure 4. 6, the current values were two orders of magnitude smaller those for the 172 nm source. However, the trend of the increase in the current with the voltage was the same as that for the 172 nm source. When the voltage exceeded 1400 V, the current increased discontinuously owing to spark discharge, resulting in damage to the photocathode. The upper limit of the stable DC discharge without spark discharge was limited to small current levels of approximately 15 µA for the 254 nm source and approximately 5 µA for the 265 nm source. The difference in the current possibly caused by the difference in the photoelectron current density of the UV light sources.

It has been reported that the work function of thin gold films is smaller than that of bulk gold. For example, the work function is 3.8 eV for thicknesses below 45 nm [79] and 4.3 eV for thicknesses below 100 nm [75]. In contrast, the work function of bulk gold is 4.9–5.45 eV

[80], [81]. The photon energies and measured power densities were 7.2 eV (172 nm) at 27 mW/cm^2, 4.88 eV (254 nm) at 0.28 mW/cm^2, and 4.68 eV (265 nm) at 9 mW/cm^2. The 172 nm excimer lamp had the highest power density with a sufficient photon energy for photoemission, even for the bulk gold surface. The power densities of the 254 nm and 265 nm UV sources were smaller than that of the 172 nm source, and the photon energies were insufficient to induce photoemission from the bulk gold surface. Even if the work function decreased because of the nanoscale thickness, the photoemission current density was affected by the small quantum efficiency. The quantum efficiency of the 15 nm thick gold thin film for transmissive photoemission at 4.6 eV was one order of magnitude smaller than at 4.9 eV [75].

The photoemission current density was the most important factor for achieving stable and continuous atmospheric-pressure gas discharge without spark discharge. An interesting result was that at 1500 V, a stable discharge current was obtained with sufficient photoemission, whereas spark discharge occurred without photoemission. The photoelectron emission current suppressed the occurrence of spark discharge. In this work, the Xe excimer lamp with sufficient photon energy and a high illumination power density was the most suitable for the photoemission-induced gas discharge.

4.4.3. Effect of the UV power density

The effect of the UV power density on the current–voltage relationship of atmospheric-pressure Ar gas discharge was examined by varying the irradiation distance between the 172 nm source and photocathode, as shown in Figure 4. 8 and Figure 4. 9. The distance between the lamp surface and quartz slide glass was varied from 0 mm (direct contact) to 9 mm. The voltage was limited below 1500 V to prevent fatal damage to the photocathode.
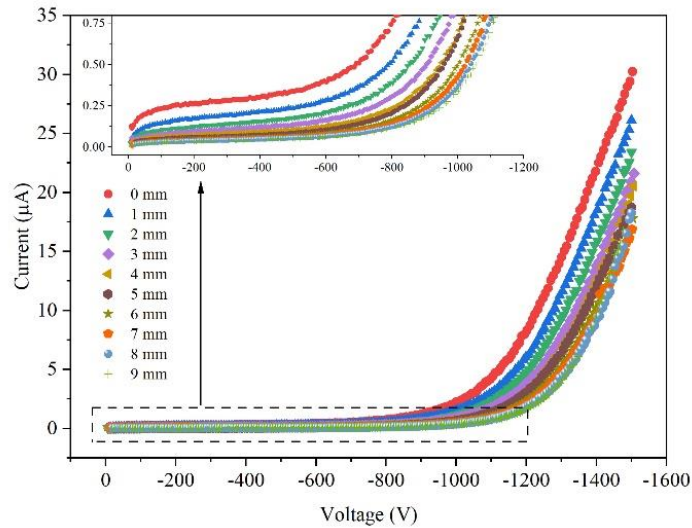
Figure 4. 8 Photoemission-induced atmospheric-pressure Ar gas discharge, current–voltage characteristics for different irradiation distances from 172 nm Xe excimer lamp.
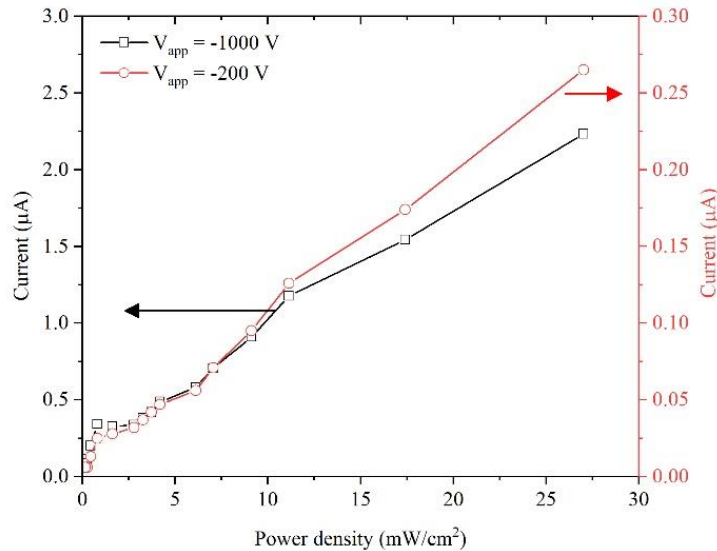
Figure 4. 9 Photoemission-induced atmospheric-pressure Ar gas discharge, current vs. UV irradiation power density.

The photoemission current in the low-voltage region (region 1 and 2) decreased as the distance increased, as shown in the inset of Figure 4. 8. Furthermore, the exponential increase in the current in the medium-voltage region (region 3) and the linear increase in the high-voltage region (region 4) parallelly moved to the high-voltage side with almost the same shapes. The shift of region 3 and region 4 can be explained by the difference in the photoemission current because of the coefficient of the exponential function.

Figure 4. 9 shows the plots of the current at 200 V, which is the photoemission current, and the current at 1000 V, where the current increases exponentially with the voltage, against the irradiated UV power density at the center. The photoemission current at 200 V and the exponentially amplified current at 1000 V depended on the UV power density. However, they were not completely proportional owing to the nonuniform profile of the UV power density and increase in the working area of the photocathode. The increase in the current due to avalanche ionization at 1000 V was almost constant at approximately 10 times. At the maximum spark-free voltage of 1500 V, the current increased not exponentially but linearly owing a resistance component, and it was not proportional to the photoemission current.

The total quantum efficiency of the 172 nm source, including the absorption coefficient (approximately 0.35) of the nanometer-thick film was estimated to be larger than 10^{-5}. The estimated quantum efficiency was close to that reported in a previous study, the quantum efficiency of a 15 nm thick gold film became saturated at approximately 10^{-4} at a photon energy of more than 4.8 eV [75] which in agreement with quantum efficiency of bulk gold [82].

4.4.4. Photoemission-induced atmospheric pressure gas discharge in air

Figure 4. 10 shows a comparison of the current–voltage characteristics obtained under Ar and air, with the same vertical (current) scale and the different horizontal (voltage) scales in the inset graph. The voltage required to approach the safe spark-free current of 30 μA was considerably higher in air (4000 V) compared to Ar (1500 V). In air, the maximum input power reached 120 mW in the discharge cell with a diameter of 15 mm and a gap length of 1 mm.

As shown in the inset of Figure 4. 10, at low voltages, the current increased almost linearly with the voltage in air, and there was no clear saturation that corresponded to the photoemission current. The linear trend in the low-voltage region (region 2) might be due to the influence of oxygen. In air, low-energy electrons had a high probability of becoming attached to oxygen; this hindered their acceleration and transport. Thus, the voltage and electric

field required to promote avalanche ionization were higher in air compared to Ar. In air, the current increased exponentially with the voltage above approximately 1500 V. At high voltages above 3500 V, the exponential increase in the current was impeded by a resistive component, like Ar case.
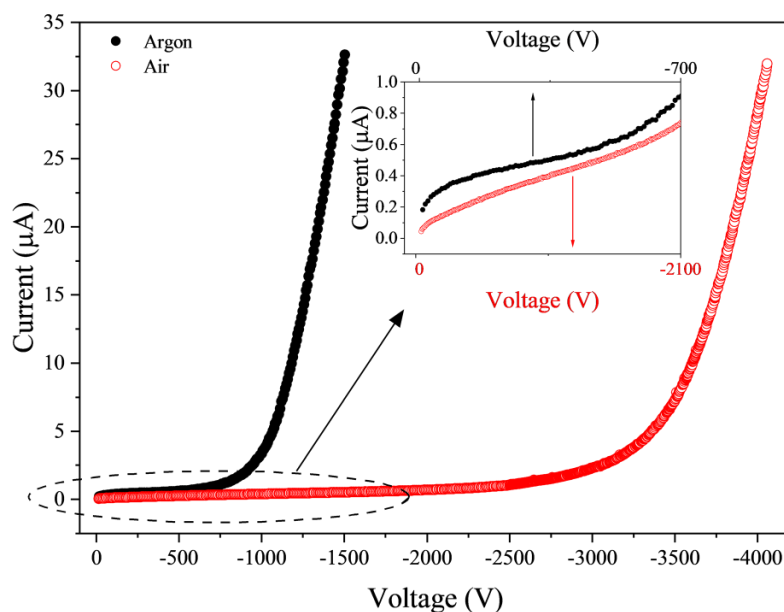
Figure 4. 10 Current–voltage characteristics of photoemission-induced (UV 172 nm) atmospheric-pressure plasma in Ar and air.

4.4.5. Optical emission spectroscopy of gas discharge

Plasma emission was expected in the discharge cell since the continuous input power, i.e., 50 mW in Ar and 120 mW in air. However, it was difficult to visually confirm the plasma emission in the cell owing to the fluorescent-UV-light-irradiated glass tube and slide glass. Thus, optical emission spectroscopy was performed to confirm the generation of plasma by the photoemission-induced discharge. Figure 4. 11 shows the typical optical emission spectra for air plasma, Ar plasma, and the Xe excimer lamp.

When the photocathode was illuminated by the Xe excimer lamp with no discharge voltage, emission peaks were observed only in the near-infrared region. There were strong peaks at 823.2 nm, 828.0 nm, 881.9 nm and weak peaks at 895.2 nm, 904.5 nm, 916.3 nm, which were assigned to Xe atomic emissions (Xe I) [83]. The vacuum ultraviolet light at 172

nm could not be observed using the spectrometer. The fluorescence of the glass could be suppressed by directing the fiber straight into the discharge cell.
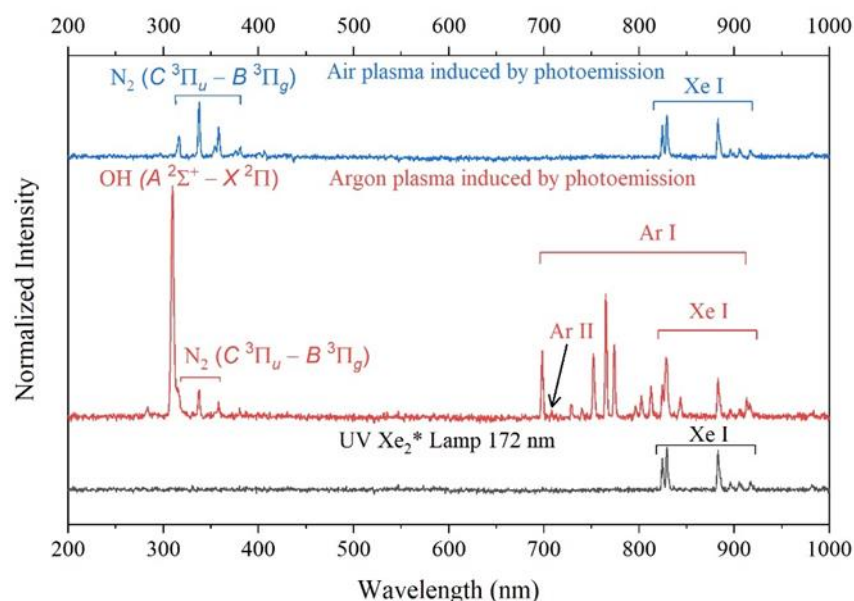
Figure 4. 11 Optical emission spectra of photoemission-induced gas discharge in Ar and air

When the discharge was operated in Ar flow at a current of 32 μA, several emission peaks appeared in addition to the Xe I emissions. At wavelengths of 698 nm–912 nm, the emission peaks for Ar atoms (Ar I) were clearly observed, with a small peak for Ar ions (Ar II) at 708 nm [83]. In the UV region, a strong emission peak for OH radicals (A-X band) at 309 nm and a series of peaks for N_2 molecules (C-B band) [83] were also detected, which were due to contaminated air in the end-opened discharge cell. In case of air plasma at a current of 50 μA, in addition to Xe I emission lines, N_2 molecule lines were detected at 315.9 nm, 337.1 nm, 358.2 nm, and 380.5 nm.

4.4.6. Gas chemical reaction analysis

Typically, atmospheric pressure plasma of air will generate both of reactive oxygen and reactive nitrogen species. To confirm the production of these species, the UV absorption spectroscopy for gas discharge was performed. The measurement was carried out in DI water with bubbling for 20 minutes continuously for each condition. Figure 4. 12 shows comparison of absorption spectra for DI water, excimer treated-DI water and gas discharge treated-DI water in atmospheric pressure environment. In case of UV only, peak around 260 nm was found

64

which correspond to ozone diluted in water peak. Moreover, tail of peak at wavelength below 220 nm was detected also. In contrast, for absorbance of atmospheric pressure gas discharge induced by UV 172 nm, beside peak at 260 nm, significant peak around 210 nm was found.

Table 4. 1 Concentration of RONS in photoemission-induced air atmospheric pressure gas
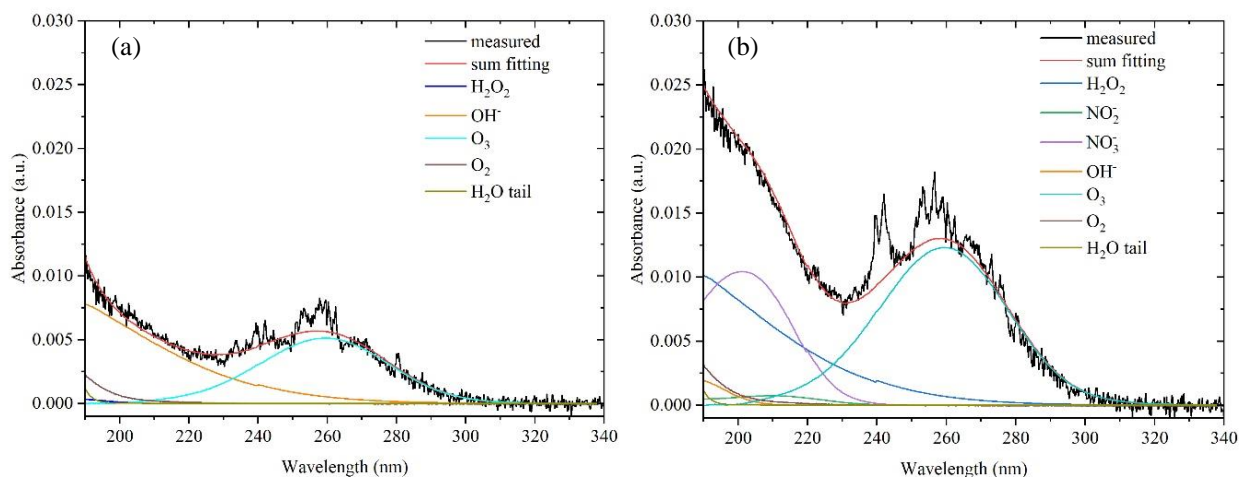
Figure 4. 12 Deconvolution of UV absorbance of (a) water-bubbled of gas-treated by UV 172 nm (b) water-bubbled of gas-treated of atmospheric pressure gas discharge induced UV 172 nm (V= 3.6 kV; I= 3.6 μA)

discharge

Reactive oxygen and nitrogen species Deconvolution results	Concentration (ppm) UV	Concentration (ppm) Photoemission-assisted gas discharge
H_2O_2	0.1	1.3
OH^-	0.005	0.03
O_3	0.05	0.12
O_2	0.04	0.06
NO_2^-	-	0.01
NO_3^-	-	0.065

To identify the details species and to estimate their concentration, deconvolution of the spectrum was performed based on the standard of our previous study [84], [85]. The deconvolution results show that, in case of UV, the absorbance spectrum consist of O_3, H_2O_2, OH, O_2 and water tail as shown in Figure 4. 12. These species are attributed as reactive oxygen species. On the other hand, NO_2, NO_3 were found in the of APP induced by UV 172 nm which correspond to nitrogen reactive species. It implies that this plasma induced chemical reaction of air and produced RONS which is key factor in medical and agriculture field.

4.5. Conclusions

Photoemission-induced atmospheric-pressure gas discharge was performed in Ar and air flowing in a discharge cell with an end opened to the atmosphere. A back-illuminated gold film with a thickness of 9 nm was used as the photocathode. Stable and continuous gas discharge was successfully achieved even in air using an excimer lamp with a wavelength of 172 nm as a UV source with a high irradiation power density and sufficient photon energy. It reached more than 30 µA at 1450 V in Ar and more than 50 µA at 4000 V in air. The use of other UV sources at the wavelength of 254 nm and 265 own in lower quantum efficiencies and power densities were also able to generate stable and continuous discharge current. However, the maximum current was limited. The current-voltage analysis indicates the occurrence of photoemission extraction and transport, then were amplified via avalanches. Optical emission spectroscopy measurement reveals in Ar gas discharge emissions of Ar atoms, OH radicals, and N_2 molecules were found, whereas, in air discharge, emissions from N_2 molecules existed. In addition, the production of RONS from gas discharge was confirmed also by measuring the UV absorbance of gas discharge.

Chapter 5. Summary

This study can be summarized as follows:

The first part of this study presents a dielectric barrier discharge plasma of Ar or N_2 mixture water-ethanol vapor for surface modification of polytetrafluorethylene (PTFE). The result shows that plasma treatment was significantly improved the wettability of PTFE. Plasma treatment with 3%, 5% and 9% ethanol diluted in Ar gas resulted in a significant reduction in the water contact angle (WCA) from 115° to $16.5 \pm 2.8°$ after 10 s of treatment. On the other hand, significant improvement of wettability was occurred when the ethanol concentration 5%, 9%, 50% and 100% diluted in N_2 gas from 115° to $11.8 \pm 2.4°$ after 10 s treatment. Furthermore, the plasma-treated PTFE experienced hydrophobic recovery after immersing in deionized water. The stable modification was achieved at WCA around 50° and 80° for Ar case and N_2 case, respectively.

An X-ray photoelectron spectroscopy was employed to analyze the chemical composition on the PTFE surface. It reveals that oxygen-containing polar groups (C–OH, C=O, and O=C–OH) were formed on the PTFE surface after plasma treatment using Ar and an additional of nitrogen-containing functional groups (C–NR and O=C–NH) after plasma treatment using N_2, reflecting the improvement of wettability. By using Ar as carrier gas, improvement of wettability was achieved by breaking the CF_2 chain and introducing oxygen-containing polar group, and simultaneously deposited a low-molecular-weight oxidized material (LMWOM) layer on the modified surface. On the other hand, in case of N_2 as carrier gas, reduction of water contact angle was induced by thin film deposition which contains oxygen-based polar groups and nitrogen-based polar groups. The thin layer deposited on the modified-PTFE surface was easily removed by deionized water, resulting in degradation of WCA.

The second part of this study reports photoemission-induced atmospheric pressure gas discharge. Photoemission-induced atmospheric-pressure DC gas discharge was successfully achieved in Ar and air using a 9 nm gold thin film deposited on quartz glass as a photocathode. The photocathode was back-illuminated with three UV light sources with wavelengths of 172 nm (Xe excimer lamp), 254 nm (Hg lamp), and 265 nm (Deep UV-LED). The continuous and stable discharge current more than 30 µA for Ar and 50 µA for air was obtained with good reproducibility at voltages below the spark-generation of 1450 V and 4000 V in Ar and air, respectively. However, the maximum current was limited for the light sources with low a photon energy and low quantum efficiency (or low power density). The current-voltage analysis suggests that discharge current can be divided into 4 regions. These regions related with the photoemission extraction, motion, and amplification via avalanche ionization. In addition, emissions from Ar atoms, OH radicals, and N_2 molecules were detected in Ar discharge and emissions from N_2 molecules in air discharge. Furthermore, analysis of reactive species production through of UV absorbance spectroscopy measurement, showed that air atmospheric pressure plasma induced by UV 172 nm produced reactive oxygen and nitrogen species (OH^-, NO_2^-, NO_3^-) which is a key point for medical application.

References

[1] P. J. Bruggeman, F. Iza, and R. Brandenburg, "Foundations of atmospheric pressure non-equilibrium plasmas," *Plasma Sources Sci. Technol*, 2017.

[2] J. Harry, "Plasmas, an Overview," *Introd. to Plasma Technol. Sci. Eng. Appl.*, pp. 1–14, 2010, doi: 10.1002/9783527632169.

[3] A. Fridman and L. A. Kennedy, *Plasma Physics and Engineering*, Second. Taylor & Francis, 2011.

[4] A. Von Keudell and V. Schulz-Von Der Gathen, "Foundations of low-temperature plasma physics - an introduction," *Plasma Sci. Technol.*, 2017.

[5] D. P. Dowling, F. T. O'Neill, S. J. Langlais, and V. J. Law, "Influence of dc pulsed atmospheric pressure plasma jet processing conditions on polymer activation," *Plasma Process. Polym.*, vol. 8, no. 8, pp. 718–727, 2011, doi: 10.1002/ppap.201000145.

[6] N. Bundaleska, D. Tsyganov, E. Tatarova, F. M. Dias, and C. M. Ferreira, "Steam reforming of ethanol into hydrogen-rich gas using microwave Ar/water 'tornado' - Type plasma," *Int. J. Hydrogen Energy*, vol. 39, no. 11, pp. 5663–5670, 2014, doi: 10.1016/j.ijhydene.2014.01.194.

[7] R. Morent, N. De Geyter, T. Desmet, P. Dubruel, and C. Leys, "Plasma surface modification of biodegradable polymers: A review," *Plasma Process. Polym.*, vol. 8, no. 3, pp. 171–190, 2011, doi: 10.1002/ppap.201000153.

[8] D. Zhou *et al.*, "Sustainable ammonia production by non-thermal plasmas: Status, mechanisms, and opportunities," *Chemical Engineering Journal*, vol. 421. Elsevier B.V., Oct. 01, 2021, doi: 10.1016/j.cej.2021.129544.

[9] T. Bernhardt, M. L. Semmler, M. Schäfer, S. Bekeschus, S. Emmert, and L. Boeckmann, "Plasma Medicine: Applications of Cold Atmospheric Pressure Plasma in Dermatology," *Oxidative Medicine and Cellular Longevity*, vol. 2019. Hindawi Limited, 2019, doi: 10.1155/2019/3873928.

[10] L. R. Winter and J. G. Chen, "N2 Fixation by Plasma-Activated Processes," *Joule*, vol. 5, no. 2. Cell Press, pp. 300–315, Feb. 17, 2021, doi: 10.1016/j.joule.2020.11.009.

[11] T. Makabe and Z. L. Petrović, *Plasma Electronics Applications in Microelectronic Device Fabrication*, Second. Taylor & Francis, 2015.

[12] M. Keidar and I. I. Beilis, *Plasma Engineering*, Second. London: Elsevier Inc., 2018.

[13] D. Xiao, *Fundamental Theory of Streamer and Leader Discharge. In: Gas Discharge and Gas Insulation. Energy and Environment Research in China, vol 6*. Berlin: Springer Berlin Heidelberg, 2016.

[14] P. Bruggeman and R. Brandenburg, "Atmospheric pressure discharge filaments and microplasmas: Physics, chemistry and diagnostics," *J. Phys. D. Appl. Phys.*, vol. 46, no. 46, Nov. 2013, doi: 10.1088/0022-3727/46/46/464001.

[15] D. Czylkowski, B. Hrycak, R. Miotk, M. Jasiński, M. Dors, and J. Mizeraczyk, "Hydrogen production by conversion of ethanol using atmospheric pressure microwave plasmas," *Int. J. Hydrogen Energy*, vol. 40, no. 40, pp. 14039–14044, 2015, doi: 10.1016/j.ijhydene.2015.06.101.

[16] K. Lotfy, "The impact of the carrier gas composition of non-thermal atmospheric pressure plasma jet for bacteria sterilization," *AIP Adv.*, vol. 10, no. 1, Jan. 2020, doi: 10.1063/1.5099923.

[17] H. Tanaka *et al.*, "State of the art in medical applications using non-thermal atmospheric pressure plasma," *Rev. Mod. Plasma Phys.*, vol. 1, no. 1, Dec. 2017, doi: 10.1007/s41614-017-0004-3.

[18] M. Keidar, K. D. Weltmann, and S. Macheret, "Fundamentals and Applications of Atmospheric Pressure Plasmas," *Journal of Applied Physics*, vol. 130, no. 8. American Institute of Physics Inc., Aug. 28, 2021, doi: 10.1063/5.0065750.

[19] Z. Chen, G. Garcia, V. Arumugaswami, and R. E. Wirz, "Cold atmospheric plasma for SARS-CoV-2 inactivation," *Phys. Fluids*, vol. 32, no. 11, 2020, doi: 10.1063/5.0031332.

[20] K. G. Kostov, "Surface modification of polymeric materials by cold atmospheric jet," *Appl. Surf. Sci.*, no. 314, pp. 367–375, 2014.

[21] J. G. Drobny, "Fluoroelastomer Composition and Properties," *Fluoroelastomers Handb.*, pp. 17–26, 2016, doi: 10.1016/b978-0-323-39480-2.00003-8.

[22] E. Dhanumalayan and G. M. Joshi, "Performance properties and applications of polytetrafluoroethylene (PTFE)—a review," *Adv. Compos. Hybrid Mater.*, vol. 1, no. 2, pp. 247–268, 2018, doi: 10.1007/s42114-018-0023-8.

[23] G. J. Puts, P. Crouse, and B. M. Ameduri, "Polytetrafluoroethylene: Synthesis and Characterization of the Original Extreme Polymer," *Chem. Rev.*, 2019, doi: 10.1021/acs.chemrev.8b00458.

[24] E. C. Dell'Orto, A. Vaccaro, and C. Riccardi, "Morphological and chemical analysis of PP film treated by Dielectric Barrier Discharge," *J. Phys. Conf. Ser.*, vol. 550, no. 1, 2014, doi: 10.1088/1742-6596/550/1/012032.

[25] J. Žigon, M. Petrič, and S. Dahle, "Dielectric barrier discharge (DBD) plasma pretreatment of lignocellulosic materials in air at atmospheric pressure for their improved wettability: A literature review," *Holzforschung*, vol. 72, no. 11, pp. 979–991, 2018, doi: 10.1515/hf-2017-0207.

[26] H. Zhang *et al.*, "Effects and mechanism of atmospheric-pressure dielectric barrier discharge cold plasma on lactate dehydrogenase (LDH) enzyme," *Sci. Rep.*, vol. 5, no. July 2018, 2015, doi: 10.1038/srep10031.

[27] C. Liu, N. Cui, N. M. D. Brown, and B. J. Meenan, "Effects of DBD plasma operating parameters on the polymer surface modification," *Surf. Coatings Technol.*, vol. 185, no. 2–3, pp. 311–320, 2004, doi: 10.1016/j.surfcoat.2004.01.024.

[28] J. Neumann, S. Brückner, W. Viöl, and C. Gerhard, "Atmospheric pressure dielectric

barrier discharge plasma-enhanced optical contact bonding of coated glass surfaces," *Appl. Sci.*, vol. 11, no. 15, Aug. 2021, doi: 10.3390/app11156755.

[29]   T. Von Woedtke, S. Emmert, H. R. Metelmann, S. Rupf, and K. D. Weltmann, "Perspectives on cold atmospheric plasma (CAP) applications in medicine," *Physics of Plasmas*, vol. 27, no. 7. American Institute of Physics Inc., Jul. 01, 2020, doi: 10.1063/5.0008093.

[30]   N. Z. A. Zabidi, S. K. Zaaba, K. D. E. Sut, C. W. S. R. Mohamad, and R. I. Masiman, "A Brief Review on Atmospheric Air Plasma," in *Journal of Physics: Conference Series*, Nov. 2021, vol. 2071, no. 1, doi: 10.1088/1742-6596/2071/1/012004.

[31]   A. Moldgy, G. Nayak, H. A. Aboubakr, S. M. Goyal, and P. J. Bruggeman, "inactivation of Virus and bacteria using cold atmospheric pressue air plasmas and the role of reactive nitrogen species," *J. Phys. D. Appl. Phys.*, vol. 53, no. 434004, 2020, [Online]. Available: https://doi.org/10.1088/1361-6463/aba066%0AManuscript.

[32]   J. M. Goddard and J. H. Hotchkiss, "Polymer surface modification for the attachment of bioactive compounds," *Prog. Polym. Sci.*, vol. 32, no. 7, pp. 698–725, 2007, doi: 10.1016/j.progpolymsci.2007.04.002.

[33]   Z. Fang, Y. Qiu, and Y. Luo, "Surface modification of polytetrafluoroethylene film using the atmospheric pressure glow discharge in air," *J. Phys. D. Appl. Phys.*, vol. 36, no. 23, pp. 2980–2985, 2003, doi: 10.1088/0022-3727/36/23/019.

[34]   C. Liu, R. D. Arnell, A. R. Gibbons, S. M. Green, L. Ren, and J. Tong, "Surface modification of PTFE by plasma treatment," *Surf. Eng.*, vol. 16, no. 3, pp. 215–217, 2000, doi: 10.1179/026708400101517161.

[35]   J. Hubert, T. Dufour, N. Vandencasteele, S. Desbief, R. Lazzaroni, and F. Reniers, "Etching processes of polytetrafluoroethylene surfaces exposed to He and He-O 2 atmospheric post-discharges," *Langmuir*, vol. 28, no. 25, pp. 9466–9474, 2012, doi: 10.1021/la300822j.

[36]   M. Shibahara, M. Akamatsu, H. Kanzaki, and K. Yamamura, "Surface Modification of Polytetrafluoroethylene Sheet by Atmospheric Pressure Plasma Treatment," *J. Surf. Finish. Soc. JapanJournal Surf. Finish. Soc. Japan*, vol. 58, no. 27, p. 420, 2007, [Online]. Available: https://doi.org/10.4139/sfj.58.420.

[37]   W. Hai, T. Hi, K. Shimizu, and T. Yajima, "Preparation of a super hydrophilic polytetrafluoroethylene surface using a gaseous ammonia-water low-temperature plasma," *J. Photopolym. Sci. Technol.*, vol. 28, no. 3, pp. 479–483, 2015, doi: 10.2494/photopolymer.28.479.

[38]   U. König, M. Nitschke, M. Pilz, F. Simon, C. Arnhold, and C. Werner, "Stability and ageing of plasma treated poly(tetrafluoroethylene) surfaces," *Colloids Surfaces B Biointerfaces*, vol. 25, no. 4, pp. 313–324, 2002, doi: 10.1016/S0927-7765(01)00333-2.

[39]   S. Zanini, R. Barni, R. Della Pergola, and C. Riccardi, "Modification of the PTFE wettability by oxygen plasma treatments: Influence of the operating parameters and investigation of the ageing behaviour," *J. Phys. D. Appl. Phys.*, vol. 47, no. 32, 2014, doi: 10.1088/0022-3727/47/32/325202.

[40] J. Nakamatsu, L. F. Delgado-Aparicio, R. Da Silva, and F. Soberon, "Ageing of plasma-treated poly(tetrafluoroethylene) surfaces," *J. Adhes. Sci. Technol.*, vol. 13, no. 7, pp. 753–761, 1999, doi: 10.1163/156856199X00983.

[41] R. Foerch, G. Kill, and M. J. Walzak, "Plasma surface modification of polyethylene: short-term vs. long-term plasma treatment," *J. Adhes. Sci. Technol.*, vol. 7, no. 10, pp. 1077–1089, 1993.

[42] A. Van Deynse, R. Morent, C. Leys, and N. De Geyter, "Influence of ethanol vapor addition on the surface modification of polyethylene in a dielectric barrier discharge," *Appl. Surf. Sci.*, vol. 419, pp. 847–859, 2017, doi: 10.1016/j.apsusc.2017.05.111.

[43] A. Van Deynse, C. Leys, R. Morent, and N. De Geyter, "Plasma Polymerization in a Nitrogen/Ethanol Dielectric Barrier Discharge: A Parameter Study," *Plasma Chem. Plasma Process.*, vol. 39, no. 5, pp. 1317–1342, 2019, doi: 10.1007/s11090-019-10007-8.

[44] M. Kehrer, A. Rottensteiner, W. Hartl, J. Duchoslav, S. Thomas, and D. Stifter, "Cold atmospheric pressure plasma treatment for adhesion improvement on polypropylene surfaces," *Surf. Coatings Technol.*, vol. 403, no. September, p. 126389, 2020, doi: 10.1016/j.surfcoat.2020.126389.

[45] A. J. Beck, Y. A. Gonzalvo, A. Pilkington, A. Yerokhin, and A. Matthews, "Positive Ion mass spectrometry during an atmospheric pressure plasma treatment of polymers," *Plasma Process. Polym.*, vol. 6, no. 8, pp. 521–529, 2009, doi: 10.1002/ppap.200800220.

[46] J. Benedikt, A. Hecimovic, D. Ellerweg, and A. Von Keudell, "Quadrupole mass spectrometry of reactive plasmas," *J. Phys. D. Appl. Phys.*, vol. 45, no. 40, 2012, doi: 10.1088/0022-3727/45/40/403001.

[47] J. Benedikt *et al.*, "Absolute OH and O radical densities in effluent of a He/H2O micro-scaled atmospheric pressure plasma jet," *Plasma Sources Sci. Technol.*, vol. 25, no. 4, 2016, doi: 10.1088/0963-0252/25/4/045013.

[48] J. Mertens, B. Nisol, J. Hubert, and F. Reniers, "Use of remote atmospheric mass spectrometry in atmospheric plasma polymerization of hydrophilic and hydrophobic coatings," *Plasma Process. Polym.*, vol. 17, no. 6, pp. 1–12, 2020, doi: 10.1002/ppap.201900250.

[49] W. E. Wallace, "Ethanol," *NIST Chemistry WebBook, SRD 69.* https://webbook.nist.gov/cgi/cbook.cgi?ID=C64175&Mask=200#copyright.

[50] B. Wang, Y. Lü, X. Zhang, and S. Hu, "Hydrogen generation from steam reforming of ethanol in dielectric barrier discharge," *J. Nat. Gas Chem.*, vol. 20, no. 2, pp. 151–154, 2011, doi: 10.1016/S1003-9953(10)60160-0.

[51] F. Chen, X. Huang, D. G. Cheng, and X. Zhan, "Hydrogen production from alcohols and ethers via cold plasma: A review," *Int. J. Hydrogen Energy*, vol. 39, no. 17, pp. 9036–9046, 2014, doi: 10.1016/j.ijhydene.2014.03.194.

[52] P. Fabbri and M. Messori, *Surface Modification of Polymers: Chemical, Physical, and Biological Routes.* Elsevier Inc., 2017.

[53] S. K. Nemani *et al.*, "Surface Modification of Polymers: Methods and Applications," *Adv. Mater. Interfaces*, vol. 5, no. 24, pp. 1–26, 2018, doi: 10.1002/admi.201801247.

[54] G. Primc, "Surface modification of polyamides by gaseous plasma—review and scientific challenges," *Polymers (Basel).*, vol. 12, no. 12, pp. 1–21, 2020, doi: 10.3390/polym12123020.

[55] E. M. Liston, L. Martinu, and M. R. Wertheimer, "Plasma surface modification of polymers for improved adhesion: A critical review," *J. Adhes. Sci. Technol.*, vol. 7, no. 10, pp. 1091–1127, 1993, doi: 10.1163/156856193X00600.

[56] G. Primc, "Recent advances in surface activation of polytetrafluoroethylene (PTFE) by gaseous plasma treatments," *Polymers (Basel).*, vol. 12, no. 10, pp. 1–7, 2020, doi: 10.3390/polym12102295.

[57] A. Sarani, A. Y. Nikiforov, N. De Geyter, R. Morent, and C. Leys, "Surface modification of polypropylene with an atmospheric pressure plasma jet sustained in argon and an argon/water vapour mixture," *Appl. Surf. Sci.*, vol. 257, no. 20, pp. 8737–8741, 2011, doi: 10.1016/j.apsusc.2011.05.071.

[58] B. E. Stein, V. Rodriguez-Santiago, A. A. Bujanda, K. E. Strawhecker, and D. D. Pappas, "Atmospheric plasma surface modification of polytetrafluoroethylene films," *Nanotechnol. 2010 Adv. Mater. CNTs, Part. Film. Compos. - Tech. Proc. 2010 NSTI Nanotechnol. Conf. Expo, NSTI-Nanotech 2010*, vol. 1, pp. 677–680, 2010.

[59] P. Luan, V. S. S. K. Kondeti, A. J. Knoll, P. J. Bruggeman, and G. S. Oehrlein, " Effect of water vapor on plasma processing at atmospheric pressure: Polymer etching and surface modification by an Ar/H 2 O plasma jet ," *J. Vac. Sci. Technol. A*, vol. 37, no. 3, p. 031305, 2019, doi: 10.1116/1.5092272.

[60] M. Kehrer, J. Duchoslav, A. Hinterreiter, A. Mehic, T. Stehrer, and D. Stifter, "Surface functionalization of polypropylene using a cold atmospheric pressure plasma jet with gas water mixtures," *Surf. Coatings Technol.*, vol. 384, no. December 2019, p. 125170, 2020, doi: 10.1016/j.surfcoat.2019.125170.

[61] C. P. Klages, "A chemical-kinetic model of DBDs in Ar-H2O mixtures," *Plasma Process. Polym.*, vol. 17, no. 8, 2020, doi: 10.1002/ppap.202000028.

[62] M. Mozetič, "Surface Modification to Improve Properties of Materials," *Materials (Basel).*, vol. 12, no. 3, p. 441, 2019, doi: 10.3390/ma12030441.

[63] N. Vandencasteele and F. Reniers, "Plasma-modified polymer surfaces: Characterization using XPS," *J. Electron Spectros. Relat. Phenomena*, vol. 178–179, no. C, pp. 394–408, 2010, doi: 10.1016/j.elspec.2009.12.003.

[64] A. Vesel, M. Mozetic, and A. Zalar, "XPS characterization of PTFE after treatment with RF oxygen and nitrogen plasma," *Surf. Interface Anal.*, vol. 40, no. 3–4, pp. 661–663, 2008, doi: 10.1002/sia.2691.

[65] G. P. López, D. G. Castner, and B. D. Ratner, "XPS O 1s binding energies for polymers containing hydroxyl, ether, ketone and ester groups," *Surf. Interface Anal.*, vol. 17, no. 5, pp. 267–272, 1991, doi: 10.1002/sia.740170508.

[66]   X. Lu, R. Stephan, M. Laroussi, and L. DaWei, *Nonequilibrium Atmospheric pressure plasma jets Fundamentals, Diagnostics, and Medical Aoolications*. Taylor & Francis, 2019.

[67]   A. Khlyustova, C. Labay, Z. Machala, M. P. Ginebra, and C. Canal, "Important parameters in plasma jets for the production of RONS in liquids for plasma medicine: A brief review," *Front. Chem. Sci. Eng.*, vol. 13, no. 2, pp. 238–252, 2019, doi: 10.1007/s11705-019-1801-8.

[68]   Z. Liu *et al.*, "Quantifying the concentration and penetration depth of long-lived RONS in plasma-activated water by UV absorption spectroscopy," *AIP Adv.*, vol. 9, no. 1, 2019, doi: 10.1063/1.5037660.

[69]   S. J. Kim and T. H. Chung, "Cold atmospheric plasma jet-generated RONS and their selective effects on normal and carcinoma cells," *Sci. Rep.*, vol. 6, no. October 2015, pp. 1–14, 2016, doi: 10.1038/srep20332.

[70]   K. Matra, H. Furuta, and A. Hatta, "DC microplasma jet for local a: C-H deposition operated in SEM chamber," *Micromachines*, vol. 8, no. 7, 2017, doi: 10.3390/mi8070211.

[71]   M. Kawata, Y. Ojiro, S. Ogawa, T. Masuzawa, K. Okano, and Y. Takakuwa, "Low-temperature synthesis of diamond films by photoemission-assisted plasma-enhanced chemical vapor deposition," *J. Vac. Sci. Technol. A Vacuum, Surfaces, Film.*, vol. 32, no. 2, p. 02B110, 2014, doi: 10.1116/1.4849355.

[72]   Y. Ohtomo, S. Ogawa, and Y. Takakuwa, "Surface morphology of a Cu substrate flattened by a 2″ photoemission-assisted ion beam source," *Surf. Interface Anal.*, vol. 44, no. 6, pp. 670–673, 2012, doi: 10.1002/sia.3863.

[73]   T. Takami *et al.*, "Catalyst-free growth of networked nanographite on Si and SiO2 substrates by photoemission-assisted plasma-enhanced chemical vapor deposition," *e-Journal Surf. Sci. Nanotechnol.*, vol. 7, no. December, pp. 882–890, 2009, doi: 10.1380/ejssnt.2009.882.

[74]   N. Kamata, S. Ajia, S. Ogawa, and Y. Takakuwa, "Suppression of electron emission from cathode in photoemission-assisted Ar plasma," *IEEE Xplore*, pp. 31–32, 2018.

[75]   X. Jiang, C. N. Berglund, and A. E. Bell, "Photoemission from gold thin films for application in multicathode arrays for electron beam lithography," *J. Vac. Sci. Technol. B Microelectron. Nanom. Struct.*, vol. 16, no. 6, pp. 3374–3379, 1998.

[76]   A. Janzen, B. Krenzer, O. Heinz, P. Zhou, D. Thien, and A. Hanisch, "A pulsed electron gun for ultrafst electron diffraction at surfaces," *Rev. Sci. Instrum.*, vol. 78, no. 013906, 2007.

[77]   Z. Tao, H. Zhang, P. M. Duxbury, M. Berz, and C. Y. Ruan, "Space charge effects in ultrafast electron diffraction and imaging," *J. Appl. Phys.*, vol. 111, no. 4, 2012, doi: 10.1063/1.3685747.

[78]   A. CĂsĂndruc, R. Bücker, G. Kassier, and R. J. Dwayne Miller, "Optical fiber-based photocathode," *Appl. Phys. Lett.*, vol. 109, no. 9, 2016, doi: 10.1063/1.4962147.

[79] T. Tsang, T. Srinivasa-Rao, and F. J., "Surface-plasmon field-enhanced multiphoton photoelectric emission from metal films," *Phys. Rev. B*, vol. 43, no. 11, pp. 8870–8878, 1991, doi: 10.1063/1.327412.

[80] M. Uda, A. Nakamura, T. Yamamoto, and Y. Fujirnoto, "Work function of polycrystalline Ag, Au and Al," *J. Electron Spectros. Relat. Phenomena*, vol. 88–91, pp. 643–648, 1998.

[81] D. E. Eastman, "Photoelectric work functions of transition, rare-earth, and noble metals," *Phys. Rev. B*, vol. 2, no. 1, pp. 1–2, 1970, doi: 10.1103/PhysRevB.2.1.

[82] W. F. Krolikowski and W. E. Spicer, "Photoemission studies of the Noble Metals. II. Gold," *Phys. Rev. B*, vol. 1, no. 2, p. 478, 1970.

[83] A. R. Striganov and N. S. Sventitskii, *Tables of spectral lines of neutral and ionized atoms*. New York: Plenum Data Corporation, 1968.

[84] J. S. Oh *et al.*, "In-situ uv absorption spectroscopy for observing dissolved ozone in water," *J. Photopolym. Sci. Technol.*, vol. 29, no. 3, pp. 427–432, 2016, doi: 10.2494/photopolymer.29.427.

[85] J. S. Oh *et al.*, "UV-vis spectroscopy study of plasma-activated water: Dependence of the chemical composition on plasma exposure time and treatment distance," *Jpn. J. Appl. Phys.*, vol. 57, no. 1, 2018, doi: 10.7567/JJAP.57.0102B9.